Revisiting Seismological Discoveries of the Inner Core

Adam T. Ringler*[1], Pritwiraj Moulik[2,3], Thomas Lee[2,4], David C. Wilson[1], and Robert E. Anthony[1]

Abstract

Seismology has been used as a tool for understanding the current physical properties of the interior of the Earth and its dynamic evolution with remarkable success over the last century. Much of this progress is due to the ever-expanding set of high-quality quantitative observations of teleseismic waveforms recorded at seismographic stations worldwide. In this work, we revisit historical seismological studies that helped first identify a core distinct in physical properties from the overlying mantle, followed by the detection of an inner core that was eventually verified to be solid based on normal-mode eigenperiods. Along with a brief overview of past studies of the Earth's inner core, we examine the reproducibility of these results and discuss how historical data compare against modern observations. After accounting for past normal-mode misidentifications, we confirm that introducing a solid inner core is required to afford significant improvements in fits to both radial modes and core-sensitive spheroidal overtones. Strong shear dissipation in the inner core of the radial reference Earth model, REM1D ($Q_\mu = 89.54$), fits the reference datasets of both normal-mode eigenperiods and quality factors accounting for physical dispersion. Because a liquid region would only have bulk dissipation, a narrow range of low Q_μ values that are preferred by the reference datasets affords additional evidence of a solid inner core. In addition, we find that there is little systematic bias in the timing accuracy of historical data, although large variances exist. Investigations into the temperature, composition, and evolution of the inner core, as well as the reproducibility of past studies, can benefit from the reconciliation of historical and modern seismological datasets.

Cite this article as Ringler, A. T., P. Moulik, T. Lee, D. C. Wilson, and R. E. Anthony (2025). Revisiting Seismological Discoveries of the Inner Core, *Seismol. Res. Lett.* **XX**, 1–20, doi: 10.1785/0220250069.

Introduction

Probing the interior structure of the Earth has been a fundamental application of seismology starting at the turn of the twentieth century. Such work arguably began with Oldham (1906), where he used the identification of two distinct travel-time curves to suggest that the interior of the Earth contains a core. Extending this work, Gutenberg (1913) was able to quantify the radius of the core to be 3471 km, an estimate remarkably close (±0.2%) to the modern reference value of 3480 km (Dziewonski and Anderson, 1981; Moulik and Ekström, 2025a,b). These pioneering works motivated the use of seismic waves from earthquakes to characterize the physical properties of the Earth. Following this line of inquiry, Lehmann (1936) provided the first unambiguous observational evidence of an inner core. Observed arrival times of core-traversing compressional waves (*PKP*) were shown to be better explained by introducing a discontinuity in the core with a radius of 1404 km and a higher compressional velocity (Fig. 1). Introducing this structural complexity also explains the core phase triplication where three distinct branches of the compressional wave (PKP_{ab}, PKP_{bc}, and PKP_{df}) follow slightly different trends based on their bottoming depths within the core (e.g., d_{bot} for *PKP* branches follow $ab < bc < df$; Fig. 2). The naming convention of PKP_{ab}, PKP_{bc}, and PKP_{df} were introduced by Jeffreys and Bullen (1940). Before this Gutenberg and Richter (1938) introduced them as P_1', P_2', and P''. For a detailed discussion on the naming convention of body-wave phases, we refer the reader to Bormann *et al.* (2013). The lack of modern seismological techniques such as ray tracing (Buland and Chapman, 1983; Crotwell *et al.*, 1999) or radially varying velocity models (Fig. 1; e.g., Dziewonski and Anderson, 1981;

1. U.S. Geological Survey, Albuquerque Seismological Laboratory, Albuquerque, New Mexico, U.S.A., https://orcid.org/0000-0002-9839-4188 (ATR); https://orcid.org/0000-0001-7089-8846 (REA); 2. Department of Geosciences, Princeton University, Princeton, New Jersey, U.S.A., https://orcid.org/0000-0002-9976-8938 (PM); https://orcid.org/0000-0002-0227-8239 (TL); 3. Lamont-Doherty Earth Observatory of Columbia University, Palisades, New York, U.S.A.; 4. Geology Department, College of Natural and Health Sciences, University of Hawai'i at Hilo, Hilo, Hawai'i, U.S.A.

*Corresponding author: aringler@usgs.gov

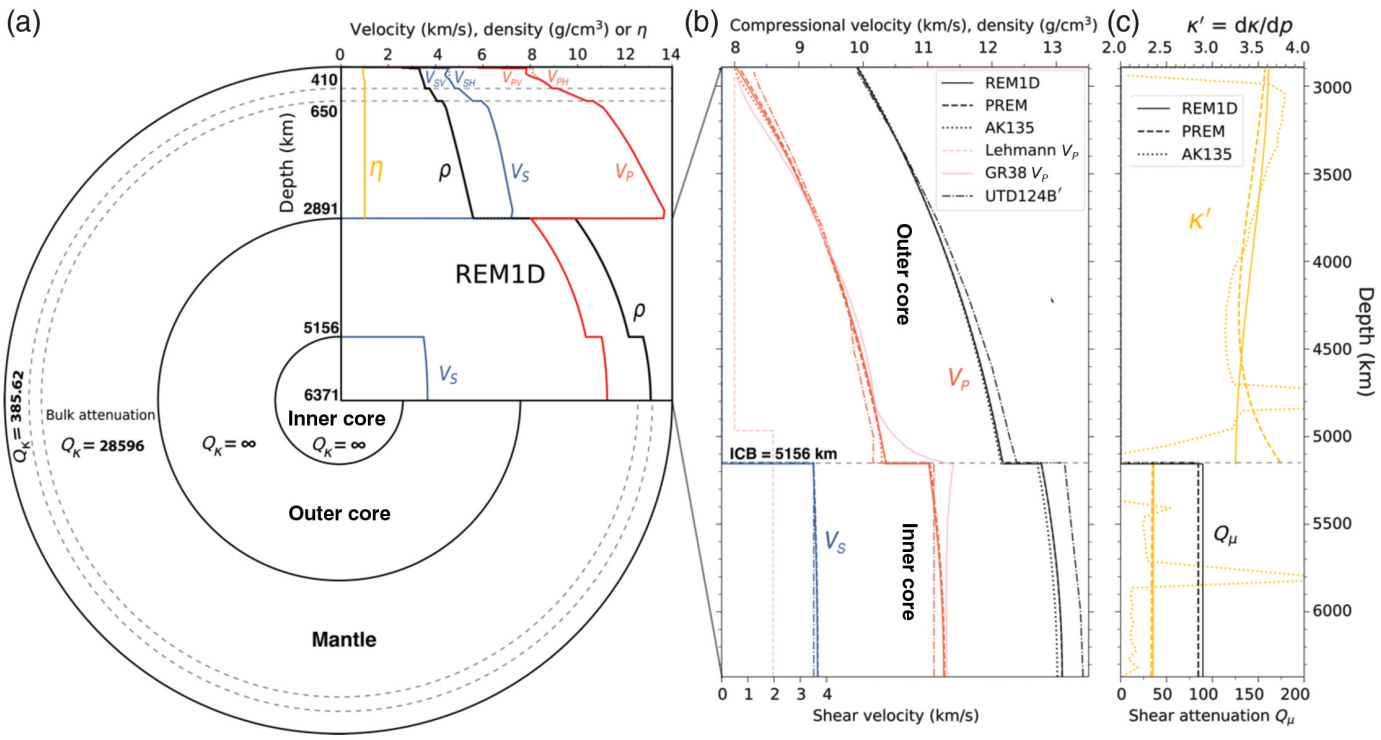

Figure 1. Core properties from the radial reference Earth model (REM1D) (Moulik and Ekström, 2025a,b). Values of radially anisotropic parameters, bulk attenuation (Q_κ), and density for (a) the whole Earth and (b) core, including Lehmann (1936), Gutenberg and Richter (1938), and Dziewonski and Gilbert (1972, UTD124B′). (c) Shear attenuation (Q_μ) and pressure derivative of bulk modulus $\kappa' = d\kappa/dp$. The ostensibly minor deviations (<1%) relative to the preliminary reference Earth model (PREM; Dziewonski and Anderson, 1981) and body-wave velocity model (AK135; Kennett *et al.*, 1995) lead to significant differences in data fits and thermochemical interpretations.

Kennett *et al.*, 1995; Moulik and Ekström, 2025a,b) complicated the testing of various hypotheses on the thermochemical state of the inner core. Despite these limitations, Gutenberg and Richter (1938) estimated the radius of the inner core to be ~1200 km, close (±1%) to the modern reference value of 1215 km (Moulik and Ekström, 2025a,b). Following this work, Birch (1940, 1952) suggested the possibility of a solid inner core and provided the possible quantitative parameters. In addition, Bullen (1950) estimated travel times for the possibility of shear waves in the inner core, which began the search for the elusive *PKJKP* phase (e.g., Okal and Cansi, 1998) that could provide direct body-wave evidence for the solidity of the inner core. However, direct observations have proven difficult because of the small amplitude of the signals (Shearer *et al.*, 2011). More recently, groups have attempted to use various stacking methods from arrays (e.g., Tkalčić *et al.*, 2022).

In the context of normal-mode theory (e.g., Dahlen and Tromp, 1998), body waves can be understood as various superpositions of spheroidal (*P–SV* phases; e.g., *PKP*) and toroidal modes (*SH* phases; e.g., *ScS*). The normal modes excited by an earthquake are categorized as spheroidal modes ${}_nS_l$ (*P–SV* motion) or toroidal modes ${}_nT_l$ (*SH* motion) with radial order n and angular order l. Large earthquakes ($M_w > 7.5$) strongly excite overtones ($n > 0$) that propagate as body waves that traverse the entire mantle and core (e.g., *PKIKP*-equivalent modes ${}_9S_0$, ${}_8S_1$). The superposition and interactions of several mode overtones that propagate with similar group velocities manifest as relatively impulsive body-wave arrivals in the time domain, which are recorded in various seismic catalogs (e.g., U.S. Geological Survey, International Seismological Centre [ISC]). In addition to identifying the arrival times of body-wave phases in time-domain seismograms, measuring the eigenperiods/eigenfrequencies and amplitude decay (e.g., quality factor Q) of the corresponding normal modes in the frequency domain is crucial for understanding the core structure.

Using normal-mode eigenperiods calculated for Earth models with either a solid or a liquid inner core and comparing them to the observations, Dziewonski and Gilbert (1971) provided observational verification of the solid inner core. Later still, the anisotropic nature of the inner core was identified using observations of anomalously split normal modes (e.g., Woodhouse *et al.*, 1986; Tromp, 1995). Although normal modes inform our understanding of the bulk properties of the inner core, much of the finer-scale structure is constrained using shorter-period body waves (<50 s dominant period; e.g., PKP_{df}, PKP_{ab}, and PKP_{bc}). Short-period body waves are used for this purpose because they are sensitive to small-scale structure and discontinuities, whereas longer-period body waves can have a Fresnel zone that is larger

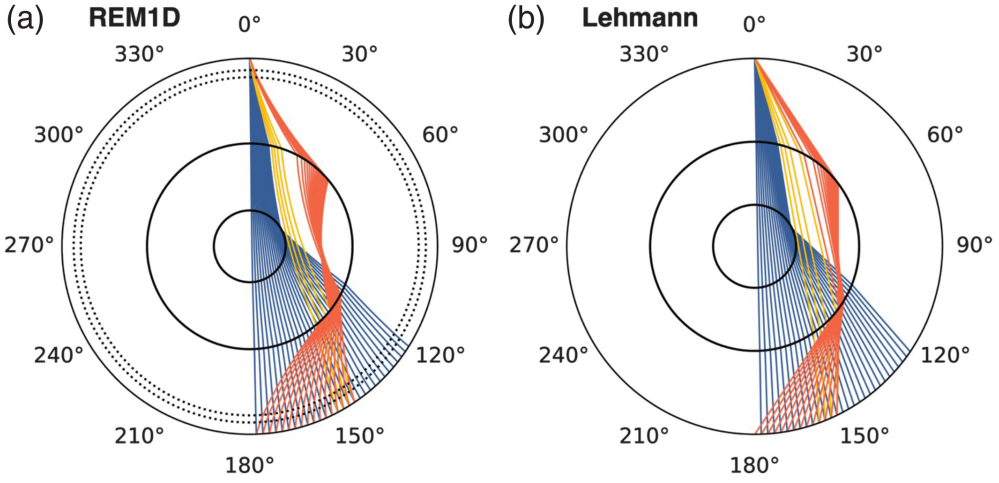

Figure 2. (a) Triplication of the core-traversing *PKP* phase. PKP_{ab} (solid red), PKP_{bc} (solid yellow), and $PKP_{df}/PKIKP$ (solid blue) through (a) the radial REM1D (Moulik and Ekström, 2025a,b). (b) Same as (a) but for the piecewise constant velocity model from Lehmann (1936). Note that the core radius is 1215 km in REM1D and 1404 km in the Lehmann model. The source lies at the surface on the equator, ellipticity is ignored, and the ray is traced at epicentral distances between 118° and 180° spaced 2° apart. Note that the body waves in the Lehmann model do not follow curved paths and $PKP_{ab/bc}$ branches bottom shallower in the outer core (4186 km depth at ~152° for bc) relative to REM1D (5075 km depth).

than the inner core (Deuss, 2014). For example, recent studies have used short-period body waves to propose 3D tomographic models of the uppermost inner core, efforts enabled by digital datasets of increasing size and quality as well as improved computational resources (e.g., Burdick *et al.*, 2019). However, even with the availability of high-quality data, some studies report using less than 10% of the available data because many records do not meet quality control criteria (e.g., Waszek and Deuss, 2013). This suggests that many studies are still relatively data-limited, as very few events meet the various quality control methods necessary to make robust observations.

Beyond understanding the thermochemical state of the inner core, seismological studies have also proposed the detection of temporal changes in the travel time of waves passing through the inner core based on several decades of global instrumentation (e.g., Song and Richards, 1996). These observations have sometimes been interpreted as changes in the rotation rate of the inner core. Such a change in relative rotation rate would imply that the inner core is not gravitationally locked to the mantle, in contrast to some dynamical expectations (e.g., Buffett, 1996). Although there are multiple data and modeling issues that could be producing inconsistencies (e.g., Tkalčić, 2024), temporal changes in the inner core would manifest as subtle signals and require very high-precision timing over long-time spans for a robust detection (Cormier *et al.*, 2021). Accurate estimation of the rotation of the inner core will require reconciliation with changes in the underlying physical properties (e.g., anisotropy or density changes; Richards, 2000; Krasnoshchekov *et al.*, 2005).

The goal of this work is to investigate the reproducibility of historical work by reviewing a few steps that led to the current understanding of the inner core and to quantify some of the limitations arising from data and processing methodologies. Instead of providing a comprehensive review, we refer the reader to Kölbl-Ebert (2001) for an overview of Lehmann (1936), while general overviews of the seismology of the core can be found in Bolt (1982), Souriau and Calvet (2015), Tkalčić (2017), and Cormier *et al.* (2021). Modern reference values of core properties based on full-spectrum tomography, which incorporates diverse astronomic–geodetic, surface-wave, normal-mode, and body-wave observations (~1–3200 s), are described by the radial reference Earth model (REM1D; Moulik and Ekström, 2025a,b). REM1D affords the average physical properties (V_P, V_S, radial anisotropy, density, shear, and bulk attenuation) of the heterogeneous Earth and serves as the update of the preliminary reference Earth model (PREM; Dziewonski and Anderson, 1981). The arrivals of major core phases (e.g., *PKIKP*) predicted by anisotropic REM1D are consistent (±0.25 s) with the isotropic body-wave model AK135 (Kennett *et al.*, 1995) that was optimized for earthquake location. Properties in the upper crust are extended to the surface, and the ocean is removed when tracing body waves through REM1D in the rest of the article. We first look at the arrival tables of Oldham (1906) and point out a curiosity in the identified phases. Next, we revisit the work of Lehmann (1936) and compare her velocity model and data to modern data, and find that much of the data provided at the time is consistent with the modern data but has a larger spread in the arrival-time residuals. We then revisit the work of Dziewonski and Gilbert (1971) and compare the historically reported mode eigenfrequencies to those estimated as part of the new reference dataset (Moulik and Ekström, 2025a). We also report new inner-core solidity experiments with shear attenuation (Q_μ) based on the quality factor (Q) measurements of normal modes. Finally, we point out some of the limitations in inner-core body-wave rotation studies when various simplifications in processing are used and how these could potentially introduce errors in the arrival times.

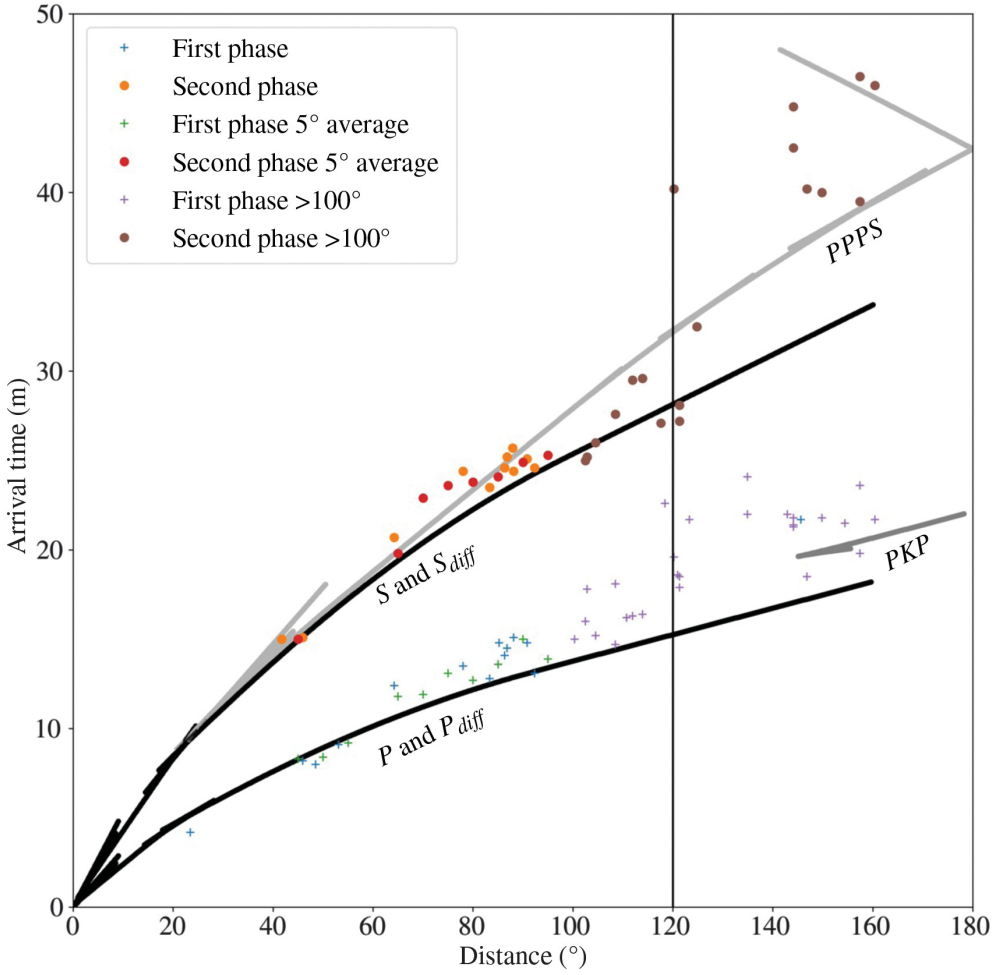

Figure 3. First arrival phases of Oldham (1906) as well as averages are shown as plus signs, and second phase arrivals are shown as circles. For reference, we have included arrival times from the radial REM1D (Moulik and Ekström, 2025a,b) for *P* and P_{diff} (black), *S* and S_{diff} (black), and *PPPS* and *PKP* (gray).

Discovery of the Core

Oldham (1906) provided seismic evidence for the existence of a core. He did this by identifying two different phase arrivals that he referred to as the first and second phase (Fig. 3), which were likely P/P_{diff} and S/S_{diff}. However, for the second phase, he also used several arrivals that were likely *PPPS* or other bounce phases that did not travel through the core. Oldham (1906) argued that the discontinuity in the second phase could be explained by the existence of a core with a slower velocity. He did not attempt to explain the composition of the core and even conceded that the data were too limited at the time to warrant further interrogation of the core.

Curiously, all the arrivals used by Oldham (1906) were consistently late relative to the modern REM1D, with a mean residual of 1.5 min for the first phase and 0.9 min for the second phase. Oldham (1906) acknowledged several possible sources of error, such as picking errors or earthquake time and location errors. It is possible that he misidentified the second phase at distances greater than 120° with that of *PPPS*, and so the discontinuity in the arrival of the second phase was not actually that of a wave that traveled through the core, but a different phase branch altogether. It is possible that his distant first phase arrivals (e.g., >140°) were *PKP* and did travel through the core along relatively straight ray paths. Oldham (1906) did suggest the possibility that the second phase was unable to travel through the core, but he rejected this in favor of the hypothesis that the core produced a slower velocity of 4.5 km/s for the second phase.

Although Oldham (1906) was data-limited due to large uncertainties in arrival times and earthquake locations, he introduced the concept of using seismic data to study the interior of the Earth and reported evidence for the existence of a core. However, we contend that his line of reasoning for the existence of the core was likely predicated on misidentified body-wave phases. Muir and Tsai (2020) also point out that the scatter in the data used in Oldham (1906) is problematic for making interpretations, and Brush (1980) pointed out that some of the data recorded at large distances are unreliable. However, this work did open the door to understanding these radial transitions in the Earth as well as the composition of various regions (Jeffreys, 1926).

The Inner Core

The discovery of the inner core was made by introducing a discontinuity that helped explain the triplicated phase branch PKP_{ab}, PKP_{bc}, and PKP_{df} (Fig. 2). Before the work of Lehmann (1936), the Earth was assumed to contain an entirely liquid core at a depth of 2900 km. Lehman calculated that no *PKP* phases would be observed with this kind of Earth model until an epicentral distance of 153.9° (e.g., orange and yellow curves in Fig. 2b). However, she noted that this conflicts with recordings of *PKP* phases at shorter distances (down to ~120°) that, due to advances in seismic instrumentation at the time,

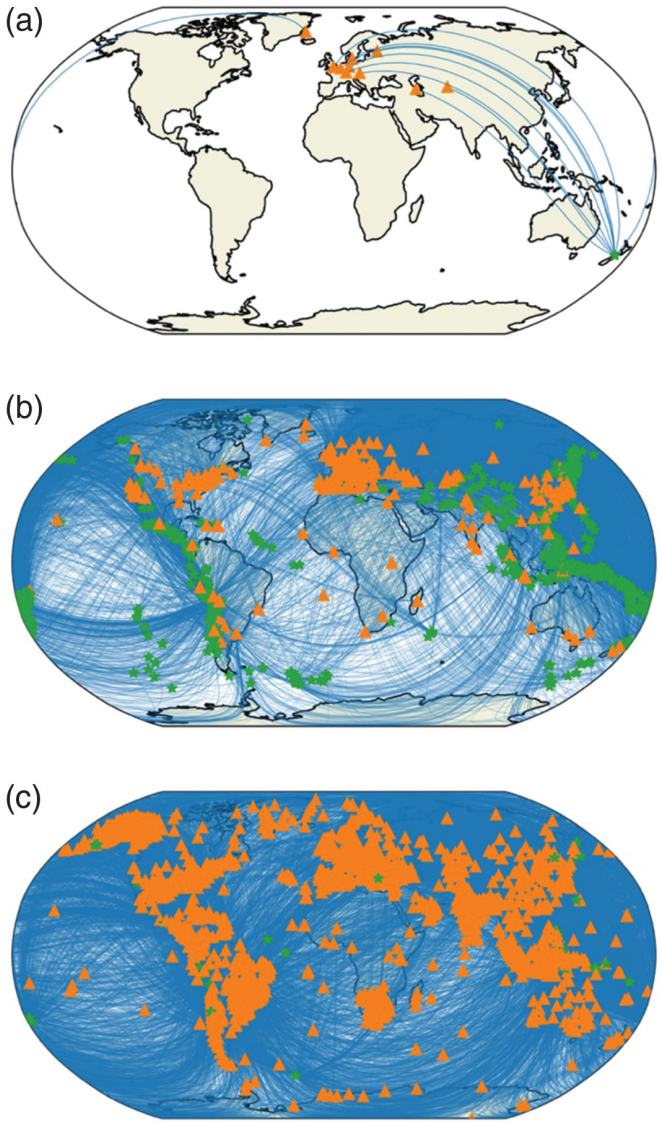

Figure 4. (a) Great-circle paths (blue) from earthquakes (green stars) to stations (orange triangles) for the 10 arrivals found in the International Seismological Centre (ISC) (ISC, 2025) bulletin used in Lehmann (1936). (b) Same as (a) but for the 7177 PKP_{df}, PKP_{ab}, and PKP_{bc} arrivals in the ISC (2025) bulletin between 1904 and 1935. (c) Same as (b) but for the 12,444 arrivals of M 7.0 and greater earthquakes between 1 January 2019 and 31 December 2021 in the ISC (2025) catalog.

had recently been observed. To explain this observation, Lehmann (1936) proposed that an inner core with a higher seismic velocity than the outer core must exist.

To evaluate this hypothesis, Lehmann (1936) studied a very limited number of high-quality records at an epicentral distance near 150° from the 1929 M_s 7.9 Murchison earthquake off the South Island of New Zealand (Fig. 4a, Table 1). We emphasize that these triplication phases are difficult to correctly identify and pick, even with modern data and the knowledge of arrival times (Fig. 5). For example, the readings identified as PKP_{df} by the ISC in the distance range from ~145° to 153° are often PKP_{bc} arrivals (Anderssen and Cleary, 1980). This is because amplitudes of PKP_{bc} arrivals are nearly an order of magnitude greater than those of $PKP_{df}/PKIKP$. After all, the latter encounters an additional reflection/transmission of energy at the inner-core boundary. In this study, we have focused on the arrival-time variations in historical studies, which are sufficiently modeled using ray theory within the distance ranges of observational interest. Although the triplication in *PKP* arrival times is well understood from ray theory, full-wave (or normal-mode) theory is necessary to interpret the intricate details of amplitude variations (e.g., Brekhovskikh, 1960; Aki and Richards, 2002).

Although Lehmann (1936) used a very limited dataset comprising 11 stations and one event (Fig. 4a), there was decent station coverage at this time with 279 stations reporting to the ISC (Fig. 4b). However, this is an order of magnitude smaller than current station coverage; 2673 stations reported the triplicated phases in the ISC (2025) catalog between 1 January 2019 and 31 December 2021 (Fig. 4c). Although Lehmann (1936) did not attempt to estimate the radius or properties of the inner core because her work was limited to explaining the PKP_{df} arrivals at short distances, her work was widely accepted and paved the way for further detailed analysis such as the radius of the inner core which was estimated only a few years later (Gutenberg and Richter, 1938). Nevertheless, she did introduce a velocity model to explain her *PKP* observations (Figs. 1b and 6). Although the absolute timing of her velocity model requires a relatively large correction of −171.83 s at a distance of 124° to match the REM1D predictions (Fig. 7), the phase branches line up relatively well, given the lack of modern ray tracing or computers at the time.

One interesting feature of the Lehmann (1936) model is an offset (3.8 s) in arrival times between *PKP* (*ab*/*bc*) and *df* (*PKIKP*) branches at ~154° due to the uniform V_P throughout the outer core in her model, which is significantly greater than the minor offset for REM1D (~0.5 s) at ~146° (Fig. 7). It is now known that the increase in velocities with depth in the outer core can be adequately expressed as second-order polynomial to fit reference datasets and match expectations from mineral physics (Moulik and Ekström, 2025a). This leads to two changes in *PKP* phases compared to Lehmann (1936): (1) ray paths curve downward till they reach a bottoming depth (d_{bot}) based on slowness/epicentral distance and relatedly; (2) they sample faster, deeper velocities and accrue less travel time (Fig. 2). Per Fermat's principle, absent gradual V_P gradients in Lehmann's model, the ray paths for *ab* and *bc* branches travel the shortest, linear path across the outer core with uniform velocity. At an epicentral distance ~152°, the *bc* branch bottoms at a relatively shallow depth of $d_{\mathrm{bot}} = 4186$ km and travels at a much slower outer-core velocity than in the "real" Earth represented by REM1D, where the ray bottoms at $d_{\mathrm{bot}} = 5075$ km. This path will be substantially different from the *df* branch in the case of Lehmann (1936), and the relative difference between inner–outer-core velocities that the two branches travel through

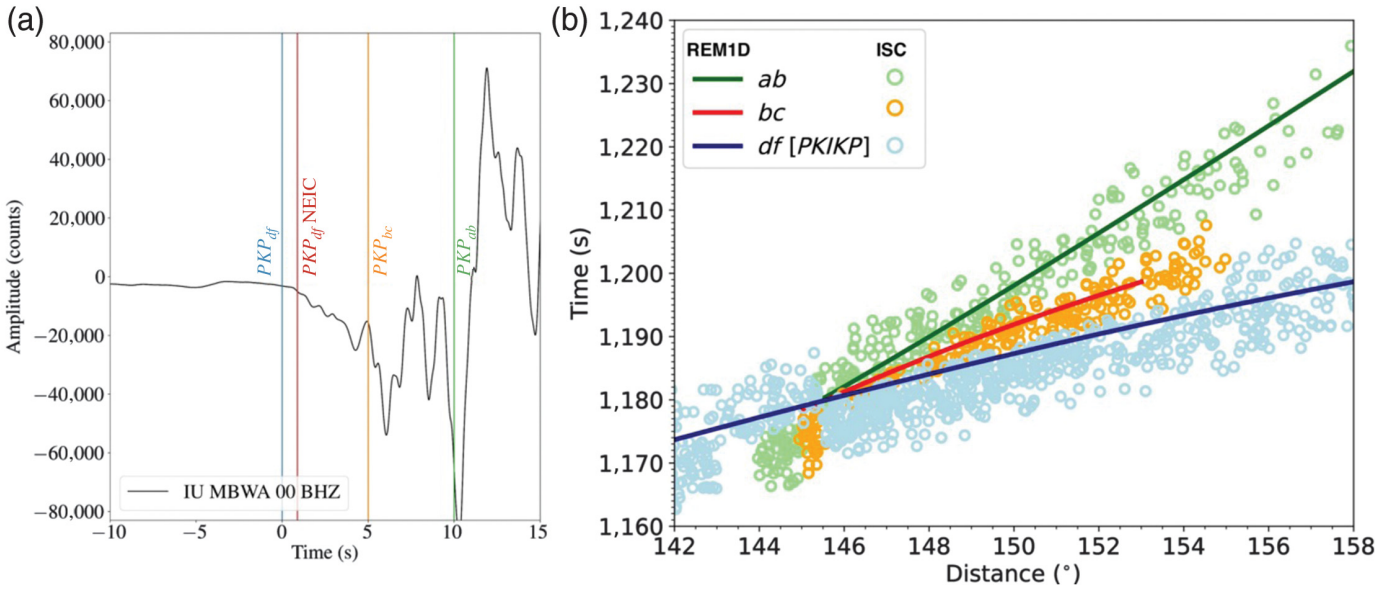

Figure 5. (a) Time-series data from the primary (location code 00) vertical-component broadband (channel BHZ) Incorporated Research Institutions for Seismology (IRIS) U.S. Geological Survey (USGS) station MBWA (Marble Bar, Western Australia) for the 26 June 2019 07:41:14.36 M_w 8.0 Peru earthquake. For reference, we have included the theoretical arrival times from the triplication PKP_{df} (blue), PKP_{bc} (orange), and PKP_{ab} (green) from radial REM1D (Moulik and Ekström, 2025a,b). Properties in the upper crust are extended to the surface, and the ocean is removed when tracing body waves through REM1D. The PKP_{df} arrival-time pick from the National Earthquake Information Center (NEIC) is shown in red. (b) ISC (ISC, 2025) travel-time picks for all earthquakes with hypocenter depths less than 20 km from 1904 to 1935, as shown in Figure 4b. REM1D travel-time branches are included for reference. It should be pointed out that during the initial picking of these phases, they would have been picked as P'.

will create an offset in arrival time. In contrast, ray paths and the outer-core V_P structure sampled by *PKP* in the REM1D model are more similar for *bc* and *df* branches, especially for the outer-core caustic at ∼146°, which leads to the minor offset in arrival time. Understandably, Lehmann (1936) was not able to resolve the details of the *PKP* triplication and V_P gradients because arrivals of only a single branch (i.e., *df* or *PKIKP*) were employed in her analysis.

TABLE 1
Phase Arrival Times from the International Seismological Centre (ISC, 2025) Bulletin Used in Lehmann (1936)

Station Code	Latitude	Longitude	Distance (°)	Arrival Time (yyyy/mm/dd hh:mm:ss.ss)	Table
SCO	70.4833	−21.95	150.51	1929/06/16 23:07:06.00	5
PUL	59.7728	30.322	150.74	1929/06/16 23:07:09.00	5
COP	55.6853	12.4325	161.07	1929/06/16 23:07:19.00	6
VIE	48.2483	16.3617	162	1929/06/16 23:07:24.00	6
GTT	51.5464	9.9642	164.66	1929/06/16 23:07:35.00	6
STR	48.5845	7.7658	167.33	1929/06/16 23:07:32.00	6
UCC	50.7983	4.3594	167.93	1929/06/16 23:07:33.00	6
KEW	51.4683	−0.3131	169.28	1929/06/16 23:07:38.00	6
IRK	52.2431	104.2711	110.78	1929/06/16 23:01:57.00	7
TAS	41.325	69.295	124.45	1929/06/16 23:06:21.00	7
BAK	40.372	49.818	137.45	1929/06/16 23:06:45.00	7

First column is the station code; the second column is the station latitude; the third column is the station longitude; the fourth column is the distance of the station to the 16 June 1929 M_s 7.9 Murchison earthquake; the fifth column is the arrival time of PKP_{df}; and the sixth column is the corresponding table in Lehmann (1936).

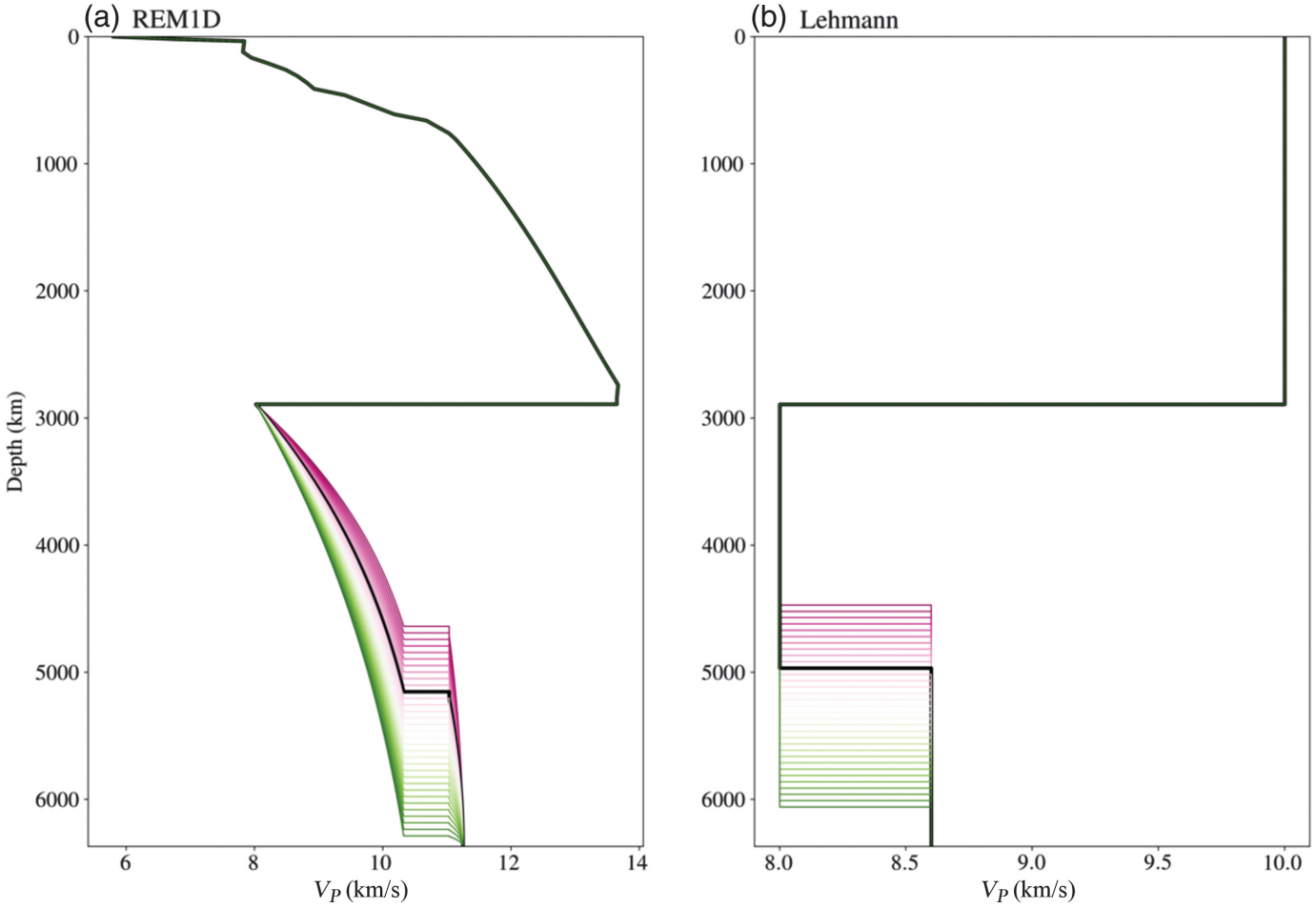

Figure 6. (a) Perturbations of the depth of the inner core and the profile of compressional velocity from radial REM1D (black; Moulik and Ekström, 2025a,b). Perturbations range from 5% shallower (pink) to 15% deeper (green). (b) Same as (a), but for the velocity model used in Lehmann (1936). The perturbed models are used to evaluate the optimal depth of the inner core based on various subsets of *PKP* datasets in Figure 8. Properties in the upper crust are extended to the surface, and the ocean is removed when tracing body waves through REM1D.

Although Lehmann (1936) used a very limited dataset of only the highest-quality records, the set of all available triplicated phases at the time is remarkably good. For example, if we perturb the REM1D inner core to fit her limited dataset (Fig. 4a) in a least-squares sense, it would yield an inner-core radius of ~1190 km, which would be ~2% deviation from the radius of 1215 km in REM1D (Fig. 8a). However, employing her piecewise constant velocity model results in a substantially larger inner-core radius that is off by more than 35% (Fig. 8b), primarily due to the trade-offs between (an overall slower outer core) velocity and (shallower) inner-core boundary while modeling arrival-time observations. Although she made use of a very limited number of stations and one earthquake, using all 7177 *PKP* phase picks available in the ISS and ISC bulletins (ISC, 2025) circa 1936 (Fig. 4b) produces a very consistent inner-core radius of 1208 km (<0.6% deviation, Fig. 8c). Note, however, that even if one assumes that Lehmann had access to the full set of bulletins, quite a feat without the data accessibility granted by modern library science and technology, processing of such a large dataset would have been difficult. Nonetheless, using about 250 events that occurred between 1918 and 1932, Gutenberg and Richter (1938) estimated the inner-core radius to be 1200 km, a result very consistent with that obtained by processing the full 1930s-era dataset with modern resources. Naturally, when a modern dataset is used, a consistent estimate of the inner-core radius is found (Fig. 8e), whereas the velocity model of Lehmann (1936) would result in an inner core with a radius ~560 km larger than modern reference values. Although the velocity models, data accessibility, and computational resources were limited at the time, given modern resources, seismologists of the 1930s would have been able to provide reasonable estimates of the inner-core radius with the datasets of the time.

We can investigate the potential biases in these datasets by looking at their statistical distributions. Figure 9 reports histograms of the residual travel times between PKP_{df}, PKP_{ab}, and PKP_{bc} picks from the ISC bulletin and those predicted from REM1D for each of the three datasets. Using the Lehmann (1936) dataset, which is composed entirely of PKP_{df} phases,

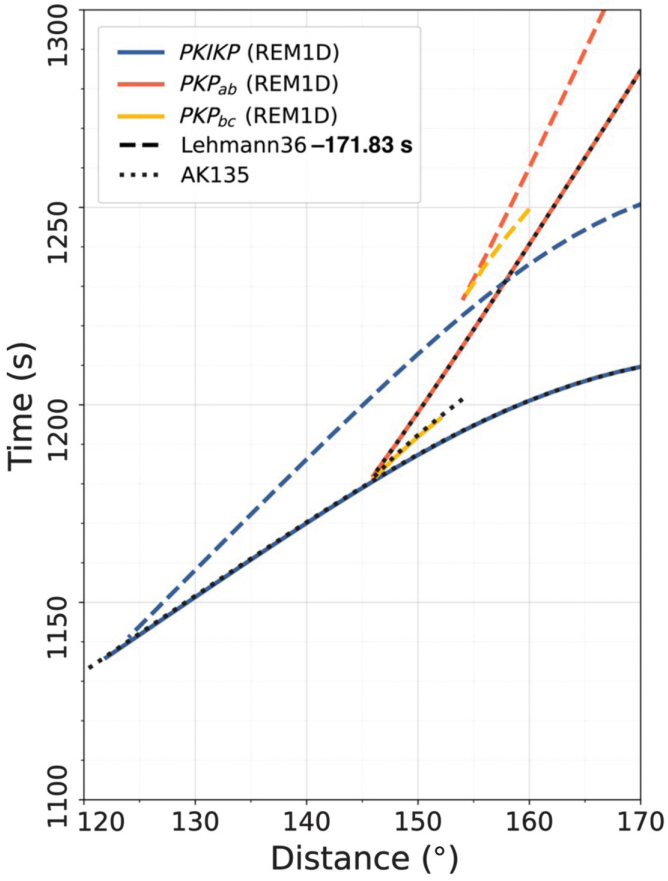

Figure 7. Arrival times as a function of distance for the triplication PKP_{ab} (solid red), PKP_{bc} (solid yellow), and PKP_{df}/*PKIKP* (solid blue) through the radial REM1D (Moulik and Ekström, 2025a,b). Arrivals (*ab*,*df*) from the anisotropic REM1D model are consistent (±0.25 s) with the isotropic body-wave model AK135 (Kennett *et al.*, 1995; black dashed). We have shifted the arrivals for the model from Lehmann (1936) by −171.83 s to match the REM1D arrival-time curve at 124°. The source is a surface-focus earthquake located at the equator, and the ellipticity correction is not applied. The large offset between *PKP*(*ab*/*bc*) and *df* (*PKIKP*) branches at ∼152° (3.8 s) is due to the constant outer-core velocity (8 km/s) in Lehmann's model (Fig. 2).

we find that the mean deviation between the expected arrival time and the observed is 4.6 s with a standard deviation of 4.1 s (Fig. 9a,d). For the historical dataset of arrivals between 1904 and 1935, we find that the mean deviation is −0.44 s with a standard deviation of 4.0 s (Fig. 9b,e). Finally, the ISC dataset from 1 January 2019 to 31 December 2020, has a mean residual of 0.029 s with a standard deviation of 1.83 s (Fig. 9c,f). The spread of the residuals suggests that there was more variance in the historical data (Fig. 9d,e) compared to modern arrival times (Fig. 9f). Although there is some systematic bias in all historical data with a mean deviation of −0.44 s (Fig. 9b,e), the spread in data is relatively large with a standard deviation of 4.03 s. It is worth noting that the mean offset of nearly 0.5 s in historical data is still enough to produce problematic residuals for modern applications like understanding the finer-scale structure of the inner core (e.g., Burdick *et al.*, 2019).

The source of arrival-time discrepancies found in the historical data could be twofold. First, picking the three phases, PKP_{df}, PKP_{ab}, and PKP_{bc} can be difficult because of the triplication, as well as their similar arrival times at certain distances (Figs. 5 and 7). Timing errors are a likely second source, including the practice of picking arrivals to the nearest 1 s, which was common in historical data (Wood, 1921). Although timing errors are still present in modern data (Ringler *et al.*, 2021), they appear to be much smaller (mean error less than 10 ms). For example, we can still see timing errors present in several ISC (2025) arrival picks (Fig. 9f). However, the systematic bias has reduced substantially in modern data, and the mean residual is only 0.029 s. This suggests that the dataset spanning 1 January 2019 to 31 December 2020 fits the radial REM1D very well, which is to be expected. The observed errors could be from stations with poor timing (e.g., Ringler *et al.*, 2021) or a misidentification of the phase. Although Lehmann (1936) mentioned only using very carefully picked arrivals, we found that the entire dataset available in ISC (2025) circa 1935 could likely have been used if sufficient computational resources were available because very few arrivals had exceptionally large outlier residuals (>5 s; Fig. 9b,e).

Many of the seismic stations used by Lehmann (1936) operated for several decades after the 1929 event used in her study. This provides an opportunity to look at changes in the mean deviation of the observed arrivals compared to the predicted arrivals as a function of time at each of these stations (Fig. 10). At a number of stations, we found decreasing residuals as a function of time. For example, station UCC (Uccle, Belgium) goes from a median residual for a decadal window centered on 1921 of 1.12–0.3 s for the decadal window centered around 2011. Looking at the medians of all stations, we note a varying but relatively constant median value (Fig. 11a). However, there is an overall trend of the standard deviations decreasing as a function of time (Fig. 11b). This suggests that observed arrival times of more recent data more closely match predicted times from the modern REM1D. Although the data before 1936 contained small systematic biases, the most dramatic improvement made in subsequent decades has been the substantial decrease in variance. Even with the improvements in accuracy, it is worth noting that even modern body-wave arrivals would not be able to identify the temperature and composition of the inner core because of their insensitivity to density structure and the difficulty in identifying phases that confirm the inner core being solid (e.g., *PKJKP*). The *PKJKP* phase is difficult to observe directly on seismograms because it loses energy when converting to the *J* phase and due to the high shear dissipation in the inner core (Shearer *et al.*, 2011), suggesting that other approaches may be necessary (e.g., arrays; Tkalčić *et al.*, 2022).

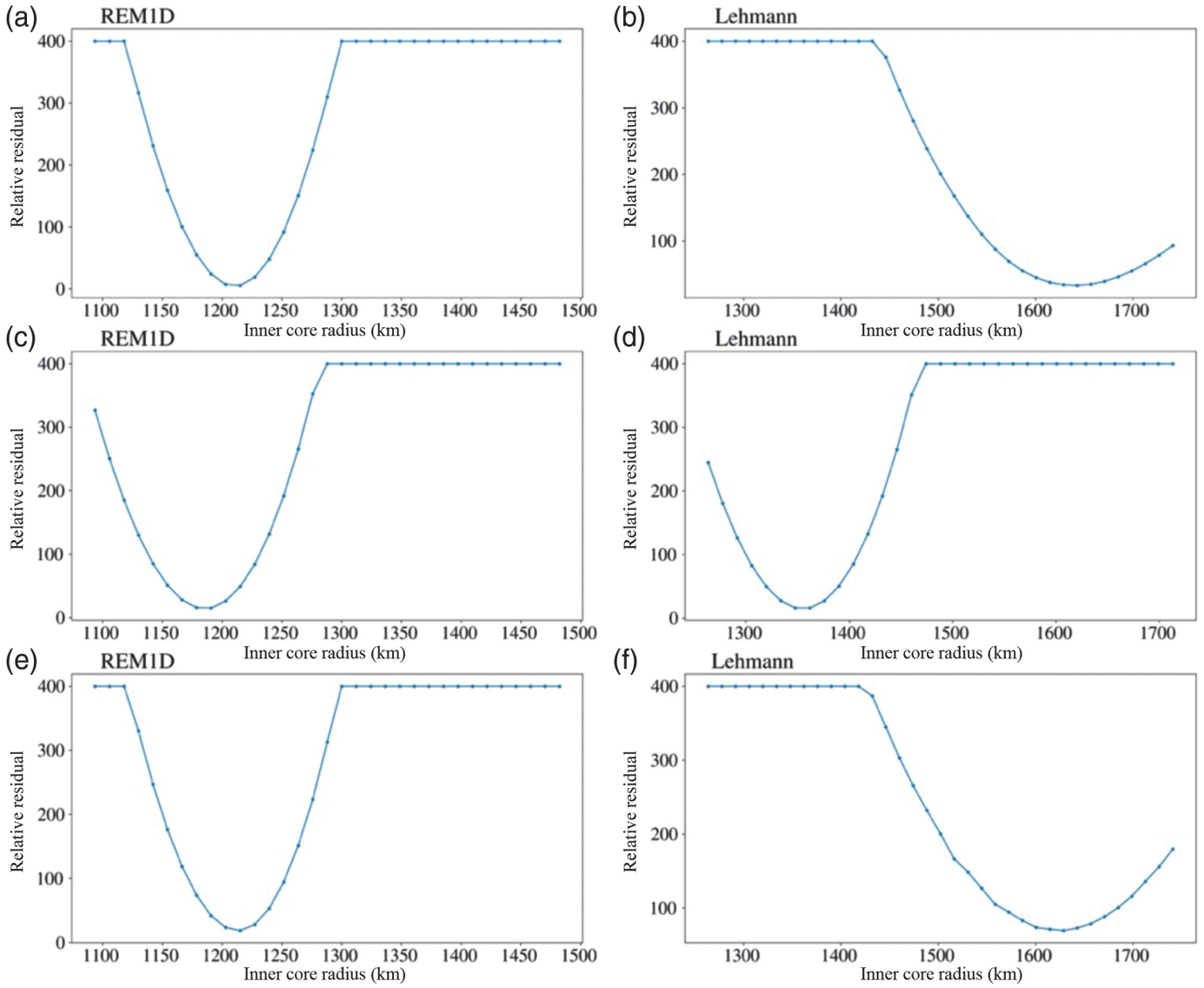

Figure 8. (a) Relative residual as a function of varying the inner-core radius of radial REM1D (Moulik and Ekström, 2025a,b) for the 11 arrivals found in the ISC (ISC, 2025) bulletin used in Lehmann (1936). (b) Same as (a) but using the velocity model from Lehmann (1936). (c) Same as (a) but for the 7177 PKP_{df}, PKP_{ab}, and PKP_{bc} arrivals in the ISC (2025) bulletin between 1904 and 1935. (d) Same as (c) but using the velocity model from Lehmann (1936). (e) Same as (c) and (f) is the same as (d) but for the 12,444 arrivals of 43 M 7.0 and greater earthquakes between 1 January 2019 and 31 December 2021 in the ISC (2025) catalog. Relative residuals are defined as the ratio of the data residual from perturbed models to that of the original velocity model (Fig. 6). Relative residuals greater than 400 have been fixed at 400 to aid interpretations.

A Solid Inner Core

After the 27 March 1964 M_w 9.2 Alaska earthquake, Dziewonski and Gilbert (1972) were able to estimate the eigenperiods/eigenfrequencies of several normal modes using analog records (digitized by hand) from stations of the WWSSN (Peterson and Hutt, 2014), a predecessor to the modern Global Seismographic Network. Based on the measurements of radial modes ${}_1S_0$, ${}_2S_0$, ${}_3S_0$, ${}_4S_0$, and spheroidal overtones ${}_2S_2$, ${}_5S_2$, ${}_6S_1$, ${}_7S_3$ ${}_8S_1$, they were able to show that the velocity model UTD124B′ with a liquid inner core was inconsistent with observations and that a solid inner core was required (Dziewonski and Gilbert, 1971). We point out that a possible piece of confusion is that the radial order n of the spheroidal-mode ${}_nS_l$ is indexed assuming no inner-core modes in Dziewonski and Gilbert (1971, 1972; Guy Masters, University of California, San Diego, personal comm., 2024). To assess this indexing issue, we calculated a dispersion diagram for the spheroidal and radial modes predicted by the radial REM1D and UTD124B′ modified to have a liquid inner core (Fig. 12). The modified UTD124B′ model does not predict the J_{SV} modes with the very high group velocities (i.e., steep slopes $d\omega/dk$ in the dispersion diagram, in which k is wavenumber) that are confined to the solid inner core in REM1D. The changes in the radial order, along with predicted mode eigenperiods from various models, are shown in

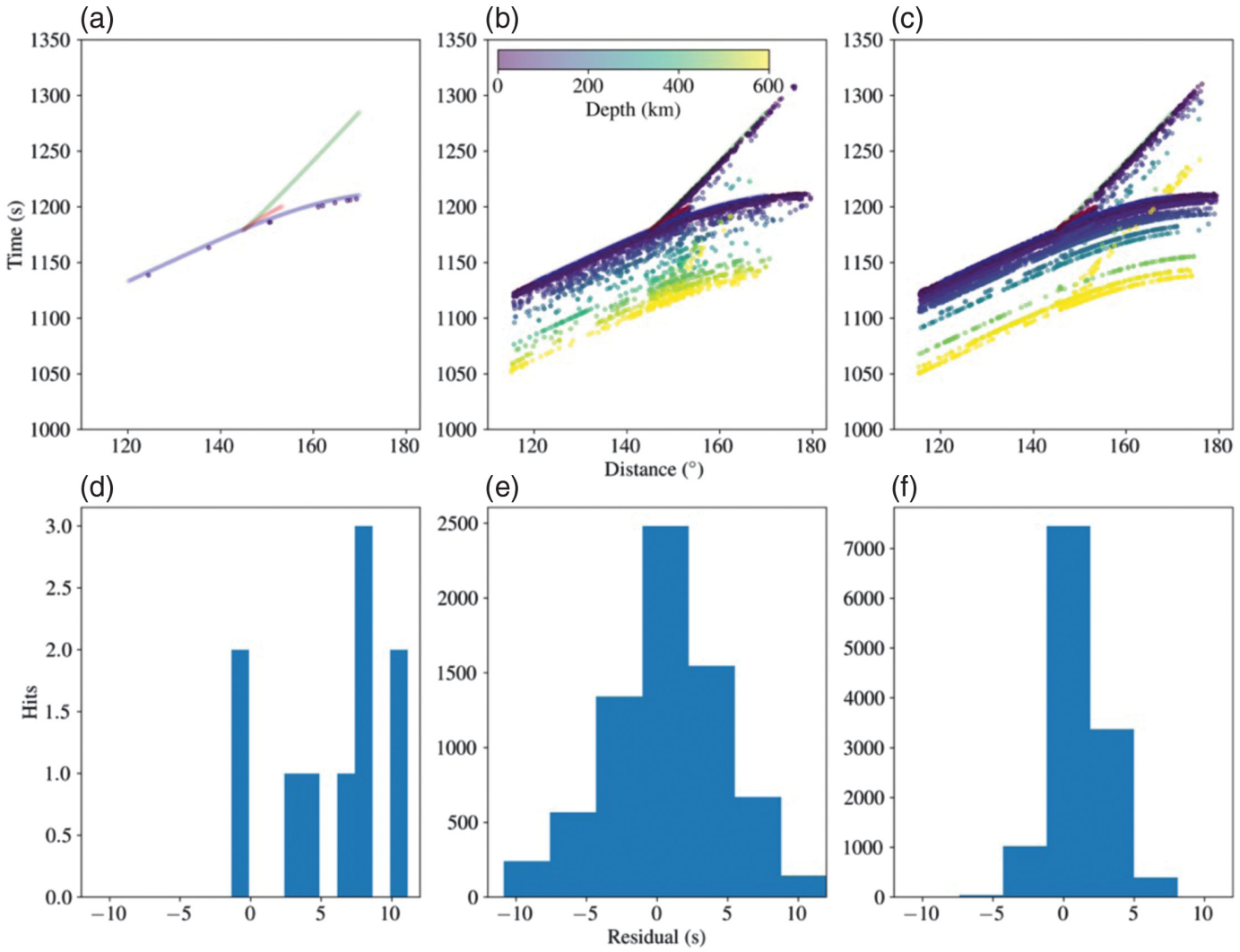

Figure 9. (a) Distances and arrival times of the phases used in Lehmann (1936) are shown in purple. The travel-time curves for PKP_{df} (blue), PKP_{ab} (green), and PKP_{bc} (red) from radial REM1D (Moulik and Ekström, 2025a,b) are also shown for reference for an event at a depth of 0 km. (b,c) Same as (a), but for the 7,177 PKP_{df}, PKP_{ab}, and PKP_{bc} arrivals in the ISC (2025) bulletin between 1904 and 1935 and for the 12,444 arrivals of M 7.0 and greater earthquakes between 1 January 2019 and 31 December 2021, in the ISC (2025) catalog, respectively. In (b) and (c), we have colored the arrival times by the depth of the event. (d) Histogram of the travel-time residuals from velocity model REM1D using the phase arrivals used in Lehmann (1936). (e) and (f) are the same as (d) but for the datasets used in (b) and (c), respectively. A zoomed-in version of (b) for shallow earthquakes is provided in Figure 5b.

Table 2; indexing with the inclusion of J_{SV} modes results in the spheroidal overtones of Dziewonski and Gilbert (1971) to correspond to ${}_3S_2$, ${}_7S_2$, ${}_8S_1$, ${}_9S_3$, and ${}_{11}S_1$ in the "real" Earth represented by REM1D. In the rest of this article, we will denote the mode from fluid inner-core models (second column of Table 2) by a prime (e.g., ${}_7S_2'$) to distinguish them from "real" Earth modes observed in the spectra of seismograms and predicted by REM1D (first column in Table 2).

Figure 13 provides the sensitivity kernels of some core-sensitive normal modes, which are functions of their displacement eigenfunctions at various depths and can be derived for the radially anisotropic REM1D model using the expressions from Mochizuki (1986). Overtone radial modes (${}_nS_0$ with $n > 0$) considered here are equivalent to radially propagating *PKIKP* waves and afford sensitivity to compressional velocity (V_P) in the whole Earth. Some spheroidal overtones are also *PKIKP* equivalent with sensitivities similar to that of the radial modes (e.g., ${}_8S_1$). When the values of the V_P sensitivity kernel are positive in the inner core, an increase in V_P within this region would cause an increase in eigenfrequencies and phase velocities and a corresponding decrease in travel time (Jeans, 1927). Note that the radial modes have large quality factors and, therefore, the decay in amplitude is substantially slower with time compared to other modes. If sufficiently long seismograms with accurate timing are available, as is the case for modern networks, the eigenperiods of these modes can be measured with high precision as reported by the new reference

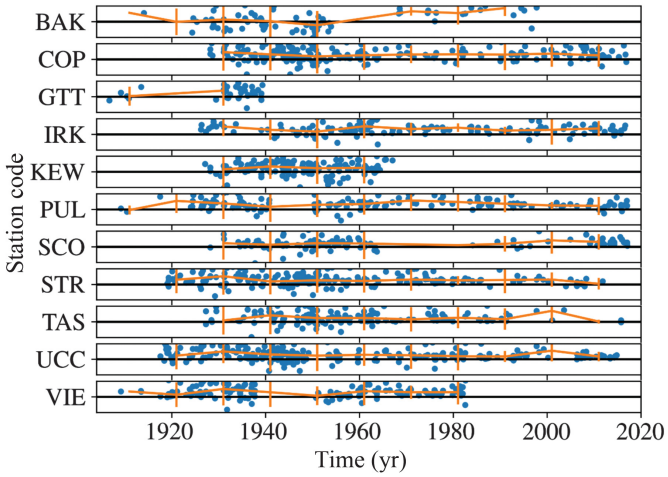

Figure 10. Station arrival-time residuals for the stations used in Lehmann (1936). The blue circles indicate individual residuals of PKP_{df} from ISC (2025) as compared to the radial REM1D (Moulik and Ekström, 2025a,b). The 10-year running medians of the arrival-time residuals, along with error bars (2.5 standard deviations), are shown in orange. The vertical window for each station is ±6 s.

dataset (Table 2; Moulik and Ekström, 2025a). This reference dataset reconciles measurements from various techniques of measuring normal-mode eigenfrequencies and quality factors, and the values are significantly different ($>2\sigma$) from the eigenperiod observations employed by Dziewonski and Gilbert (1971, 1972).

Some observed eigenfrequencies in fluid-core models by Dziewonski and Gilbert (1971) were indexed as ${}_2S_2'$ and ${}_7S_3'$, which correspond to ${}_3S_2$ and ${}_9S_3$ in models with a solid inner core. In the "real" Earth, ${}_2S_2$ and ${}_7S_3$ are J_{SV}-equivalent modes (i.e., similar in character to *PKJKP*, *SKJKS*, or *SKSKP*) and are predominantly sensitive to the shear wavespeed in the solid inner core (Fig. 13). Because J_{SV}-equivalent modes are difficult to measure due to the limited displacements at the surface, these two modes were not used in the construction of the PREM model (Dziewonski and Anderson, 1981) around a decade later, and remain excluded from the modern reference dataset and the radial REM1D. Based on the mode-ray duality, the low surface displacements of these overtone modes provide an explanation why the detection of related body-wave phases that traverse the inner core as shear waves (e.g., *PKJKP*) has remained elusive in observational seismology. Although techniques are being developed to iteratively fit spectra and glean information on these kinds of modes through coupling/resonance with other modes, these are strongly nonlinear inversions that require good starting source mechanisms and REM1Ds that have only materialized relatively recently.

Based on our calculations of modes for various inner-core scenarios, we found that ${}_7S_1'$ and ${}_9S_1'$ in fluid-core models were misidentified as ${}_6S_1'$ and ${}_8S_1'$, respectively by Dziewonski and Gilbert (1971, 1972). Throughout the article, we use ${}_nS_l'$ to denote a spheroidal mode of radial order n and angular degree l as produced by a model with a fluid core. This is evident based on our calculated eigenperiods of ${}_6S_1'$ and ${}_8S_1'$ for a modified liquid-core UTD124B′ model, which are substantially different (>50 s) from the reported eigenperiods (compare with table 1 in Dziewonski and Gilbert, 1971), while predictions for ${}_7S_1'$ and ${}_9S_1'$ are more consistent. The corresponding modes in the "real" Earth with a solid inner core are ${}_8S_1$ and ${}_{11}S_1$, respectively (Fig. 12, Table 2). It is worth noting that Dziewonski and Gilbert (1971, 1972) reported the eigenperiods of the appropriately indexed mode for solid inner-core scenarios, even though only the modes indexed with fluid inner cores are listed, albeit with the misidentification of ${}_6S_1'$ and ${}_8S_1'$. The use of correct modes for both solid/liquid inner-core scenarios helps us reproduce the trends in their reported calculations (compare with table 1 in Dziewonski and Gilbert, 1971). We document this explicitly in Table 2 to hopefully help future readers avoid this confusion.

Given the issues with the mode identification and quality of measurements employed by Dziewonski and Gilbert (1971, 1972) for their validation of a solid inner core, we reinvestigate their results using modern reference datasets and models. We calculate the eigenperiods for the modes used in Dziewonski and Gilbert (1972) for several radial models, first with a solid inner core (UTD124B′, PREM, and REM1D), and then with a liquid inner core ($V_S = 0$, $Q_\mu = 0$) retaining other parameters elsewhere in the Earth (Table 2). We find that the chi-square misfit between the reference dataset (Moulik and Ekström, 2025a) and the eigenperiods predicted by REM1D with the solid inner core ($\chi^2/N = 200$) is significantly lower than for a liquid inner core ($\chi^2/N \sim 500{,}000$), which is significant at the 99% confidence level. Only contemporary models with a solid inner core (PREM, REM1D) afford reasonable fits ($\chi^2/N \leq 200$) to the modern reference measurements of the "real" Earth modes employed by Dziewonski and Gilbert (1971).

Starting from a model with a solid outer core, the rigidity may be decreased to approach a zero value should observations require it. Several spheroidal overtones (${}_8S_1$, ${}_{11}S_1$) and radial modes are mostly compressional energy with some negative kernel values for inner-core V_S perturbations; these types of modes were categorized as group I by Dziewonski and Gilbert (1971, 1972) and would show an increase in eigenfrequency (and decrease in eigenperiod) as $V_S \to 0$ (Fig. 13). In contrast, eigenperiods of the other spheroidal overtones (group 2) would increase for a liquid inner core (Table 2). The only way to reverse the trend in eigenperiods due to $V_S \to 0$ is to reduce inner-core density relative to outer core for group 1 modes and increase the V_P (or bulk modulus) for group 2 modes (i.e., positive kernels in Fig. 13). The former scenario can be disfavored based on purely physical considerations, whereas the latter leads to inconsistencies with body-wave phases that

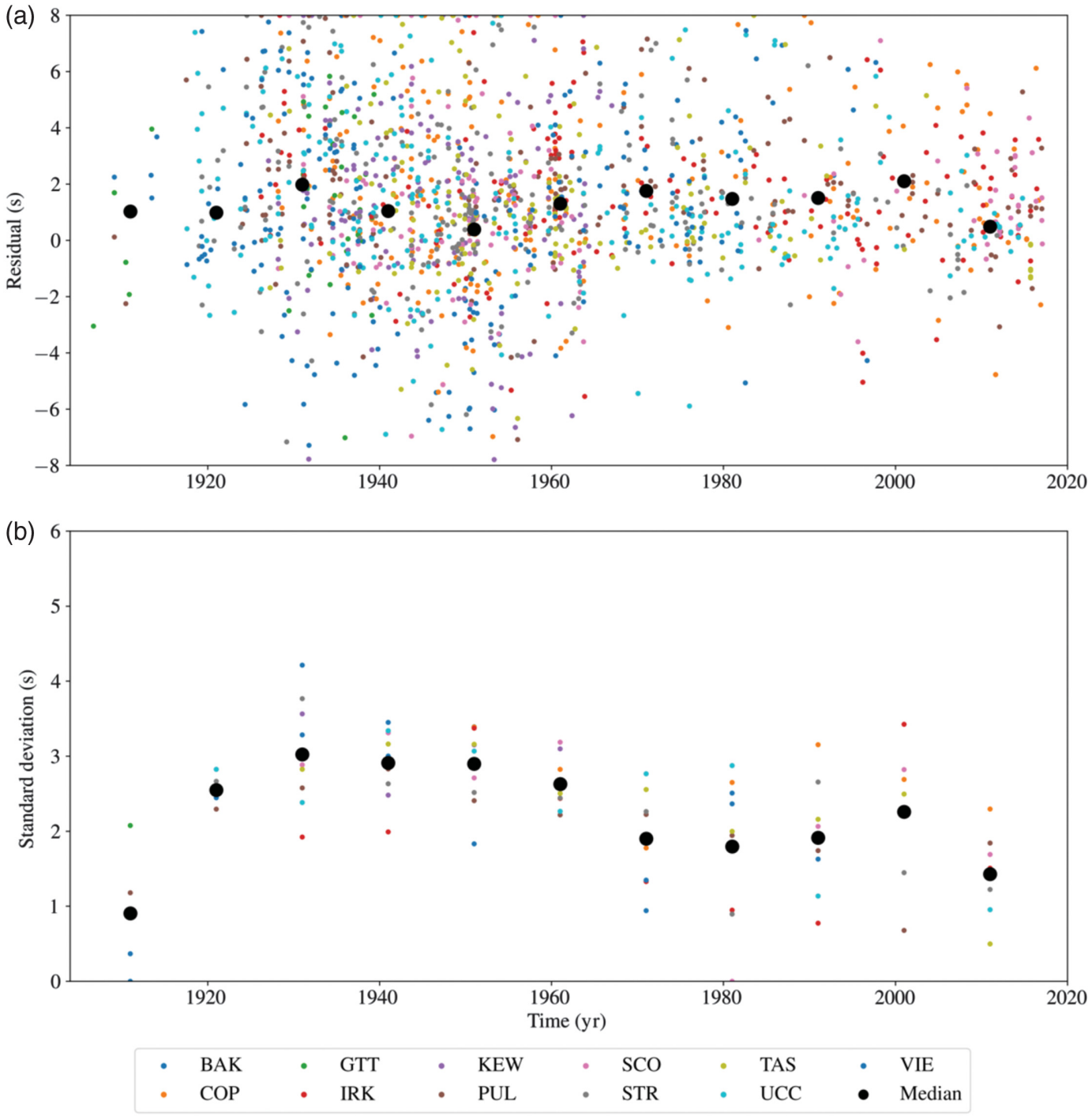

Figure 11. (a) Residuals from arrival times of PKP_{df} from the ISC (2025) as compared to the radial REM1D (Moulik and Ekström, 2025a,b) for the stations used in Lehmann (1936), which are listed in the legend. The black circle denotes the median of all stations using the 10-year medians of the mean values for each station. (b) Standard deviations using 10-year windows for each station. The median of the year windows for all stations is shown in black.

constrain the V_P structure in the inner core relatively well. Based on this trade-off during the fitting process, the basic premise of Dziewonski and Gilbert (1971, 1972) still holds true that jointly fitting the radial modes and inner-core sensitive spheroidal overtones requires invoking a solid inner core with nonzero values of V_S and shear modulus μ. It can be confusing to a reader that Dziewonski and Gilbert (1971, 1972) discuss the sensitivities of J_{SV} modes ${}_2S_2$ and ${}_7S_3$ that are not readily observed to support their solid inner-core arguments; the issue becomes clearer when their observations are attributed instead to the fluid-core modes ${}_2S_2'$ and ${}_7S_3'$ that correspond to ${}_3S_2$ and ${}_9S_3$ in the "real" Earth. Even in the absence of direct eigenperiod measurements of J_{SV} modes, other spheroidal overtones identified in our group 2 category (e.g., ${}_7S_2$) also have strong positive

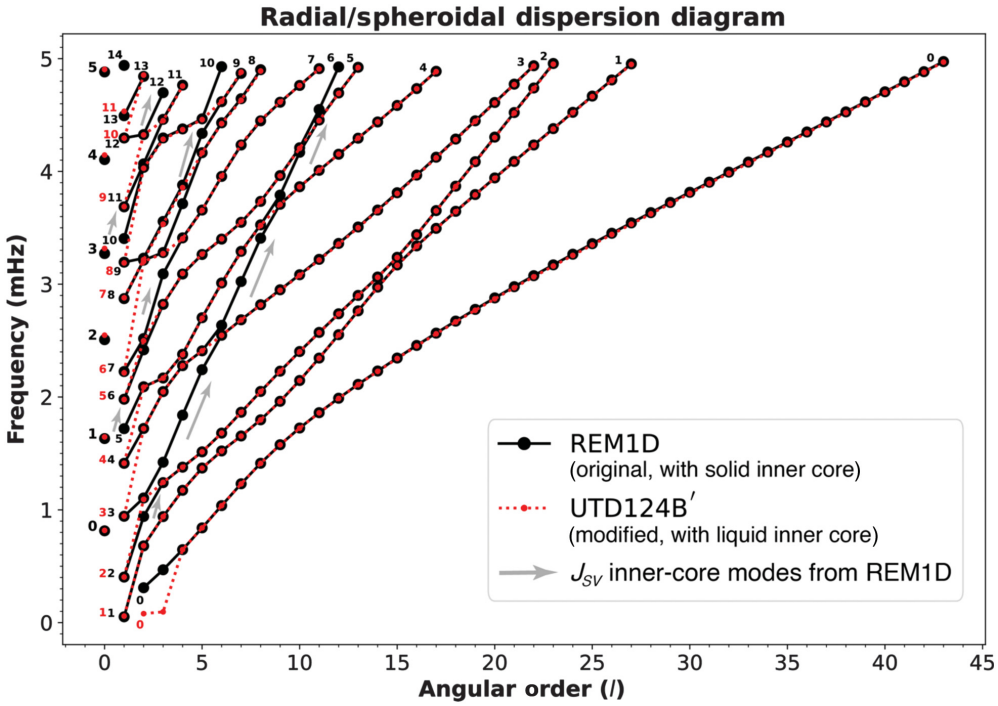

Figure 12. Dispersion diagram showing the spheroidal and radial modes predicted by the radial REM1D (Moulik and Ekström, 2025a,b), All ${}_nS_l$ modes below 5 mHz (eigenperiods > 200 s) are plotted versus the angular order l. Small numbers of left label denote the radial modes ($l = 0$) and the repeated numbers 0–14 denote the low-frequency and high-frequency ends of various overtone branches (n). Note that the modified UTD124B′ model with a liquid inner core (compare with table 1 in Dziewonski and Gilbert, 1971) does not predict the J_{SV} waves with the very high group velocities (i.e., slopes $d\omega/dk$) that are confined to the solid inner core in REM1D. Correct indexing with the inclusion of J_{SV} modes helps identify misidentified modes (Table 2).

V_S kernels in the inner core albeit with additional sensitivity to shallower structure (Fig. 13). In conjunction with other complementary datasets such as surface waves and body waves, the modern radial REM1D is able to exclude trade-offs with shallow sensitivities and robustly constrain the inner-core variations (Moulik and Ekström, 2025a,b).

Since Dziewonski and Gilbert (1972) started their work on verifying the solidity of the inner core with a starting model in which the inner core was solid, sensitivity kernels of misidentified spectral peaks (e.g., ${}_6S_1'$ and ${}_8S_1'$) would influence the structural inversion. For example, the misidentification and structural modeling of ${}_8S_1$ in observed spectra as ${}_6S_1'$ in liquid-core models (in lieu of ${}_7S_1'$) by Dziewonski and Gilbert (1971) may explain the substantially larger residuals from UTD124B′ ($\chi = -55$) compared to REM1D ($\chi = -8$). Conflating two modes with different structural sensitivities during identification from waveform spectra can lead to large data residuals. In addition, these calculations were all done before Woodhouse (1976) suggested a correction to Backus and Gilbert (1968) for normal-mode frequency and perturbation calculations. This historical error in perturbation theory could have led Dziewonski and Gilbert (1971, 1972) to inaccurately assess their resolving power and attribute data residuals to a less-than-optimal structure. However, as outlined by Woodhouse (1976), the normal modes for the derived models (e.g., with solid and liquid inner cores) could be solved by a direct calculation (e.g., Fig. 12) and checked for data fits (e.g., Table 2), so it is very unlikely there were gross errors in historical studies due to this past issue in perturbation theory.

It is now possible to look at the attenuation of core-sensitive modes, which would have been difficult in historical studies because of the limited instrumentation. Modern studies agree on a relatively high amount of shear dissipation in the inner core ($Q_\mu \sim 90$–100) based on the amplitude decay of radial and other *PKIKP*-equivalent modes (e.g., Widmer *et al.*, 1991; Moulik and Ekström, 2025b). An even more dissipative inner core would correspond to the high-attenuation limit $1/Q_\mu \to \infty$ (or $Q_\mu \to 0$) and reduce the velocity "sensed" by a long-period normal mode ($V_S \to 0$) even in case of slight rigidity (nonzero V_S and μ at the reference period of 1 s) due to physical dispersion in an anisotropic region (compare with equation 8 in Moulik and Ekström, 2025b). Figure 14 extends the inversion results in Moulik and Ekström (2025b) by performing a grid search around the reference $Q_\mu = 89.54$ in the REM1D inner core. Because of physical dispersion, a perturbed V_S profile that differs by up to ~150 m/s from the REM1D profile (valid at the reference period of 1 s) is "seen" by core-sensitive modes with longer eigenperiods (~400 s for ${}_7S_2$).

Figure 15 reports the chi-square misfits of the reference datasets from Moulik and Ekström (2025a) to scenarios that either suppress (higher Q_μ) or accentuate (lower Q_μ) the amount of shear dissipation in the inner core (Fig. 14). The optimal range of Q_μ, which corresponds to the minima in misfits for all modes and the subset of core-sensitive spheroidal overtones, is consistent with REM1D estimates. Both lower and higher dissipation than REM1D in the inner core leads to deterioration of fits to eigenperiods and quality factors. The significant deterioration in fits of eigenfrequencies (up to ~1000 times in Fig. 15), due to the relatively minor reduction

TABLE 2
Eigenperiods of Normal Modes Used in Dziewonski and Gilbert (1971)

"Real" Earth Solid IC Mode	D and G (1971) Liquid-Core Mode	D and G (1971) Observed	Reference Observation ± Uncertainty	Solid Inner Core (Column I, ${}_nS_l$)			Liquid Inner Core (Column II, ${}_nS_l$)		
				UTD124B′ [χ]	PREM [χ]	REM1D [χ]	UTD124B′ [χ]	PREM [χ]	REM1D [χ]
${}_1S_0$	${}_1S_0'$	613.57 s	612.925 ± 0.030 s	614.64 s [−57]	612.87 s [2]	612.77 s[5]	607.44 s [183]	605.57 s [245]	605.47 s [249]
${}_2S_0$	${}_2S_0'$	398.54 s	398.579 ± 0.084 s	397.70 s [10]	398.27 s [4]	398.64 s [−0.7]	392.42 s [73]	392.77 s [69]	393.16 s [65]
${}_3S_0$	${}_3S_0'$	305.84 s	305.571 ± 0.003 s	306.11 s [−181]	305.66 s [−28]	305.63 s [−20]	301.48 s [1365]	300.83 s [1580]	300.80 s [1592]
${}_4S_0$	${}_4S_0'$	243.95 s	243.518 ± 0.002 s	243.92 s [−203]	243.55 s [−16]	243.59 s [−35]	241.23 s [1143]	240.78 s [1370]	240.80 s [1358]
${}_3S_2$	${}_2S_2'$	904.23 s	904.037 ± 0.106 s	904.54 [−5]	904.08 s [−0.4]	904.85 s [−8]	915.08 s [−104]	914.45 s [−98]	915.40 s [−107]
${}_7S_2$	${}_5S_2'$	397.36 s	396.723 ± 0.129 s	397.24 [−4]	397.25 s [−4]	397.07 s [−3]	400.18 s [−27]	399.64 s [−23]	399.49 s [−21]
${}_8S_1$	${}_7S_1'\{{}_{16}S_1'\}$	348.41 s	348.117 ± 0.006 s	348.45 [−55]	348.04 s [12]	348.16 s [−8]	347.33 s [132]	346.85 s [211]	347.02 s [183]
${}_9S_3$	${}_7S_3'$	281.37 s	281.174 ± 0.015 s	281.80 [−42]	281.34 s [−11]	281.19 s [−1]	282.99 s [−121]	282.38 s [−81]	282.26 s [−72]
${}_{11}S_1$	${}_9S_1'\{{}_{18}S_1'\}$	272.10 s	271.172 ± 0.043 s	271.97 [−19]	271.34 s [−4]	271.30 s [−3]	271.19 s [−0.4]	270.42 s [18]	270.43 s [17]
			χ^2/N =	9,195	154	200	361,213	500,000	499,448

Predictions by reference Earth model (REM1D) (Moulik and Ekström, 2025a,b) and historical models (${}_nS_l$), and with the introduction of a liquid inner core (${}_nS_l$). Mean chi-square fit χ^2/N in which $\chi = [T_{obs} - T_{pred}]/\sigma$ for this subset ($N = 9$) of reference observations from REM1D. Modes misidentified by Dziewonski and Gilbert (1971) are denoted within {}. PREM, preliminary reference Earth model.

in V_S (~150 m/s) associated with reduction in Q_μ (Fig. 14), is consistent with the orders of magnitude deterioration in data fits at the end limit of a fluid inner core ($V_S = Q_\mu = 0$; Table 2). The strong shear attenuation in the REM1D inner core is constrained well based on our experiments ($Q_\mu = 89.54$; Fig. 15) and has important implications for the dominant mechanism of energy dissipation in this region that needs to be explored in future work. Note that the substantial changes in fits to eigenperiods are purely due to physical dispersion caused by shear dissipation because velocity/density structure is fixed at REM1D values in this experiment. Fits afforded by PREM are significantly worse for all core-sensitive datasets; a detailed comparison between REM1D and other radial models is provided elsewhere (compare with section 2.4 and table 2 in Moulik and Ekström, 2025b).

Reference Properties of the Core

Modern estimates of the average physical properties in the inner core are reported by REM1D (Fig. 1; Moulik and Ekström, 2025a,b). REM1D is constructed using a new reference dataset comprising normal-mode eigenfrequencies and quality factors, surface-wave dispersion curves, impedance constraints, and travel-time curves from body waves, and astronomic–geodetic observations. The inner core is a principal region that is 1215 km in radius (depth 5156–6371 km) with physical properties that increase with depth as a polynomial up to order 3. The range of REM1D physical properties in the inner core is compressional velocity ($V_P \sim 11.02$–11.25 km/s), shear velocity ($V_S \sim 3.49$–3.66 km/s), density ($\rho \sim 12.77$–13.09 g/cc), and a constant shear attenuation ($Q_\mu = 89.54$). REM1D accounts for the intertwined aspects of (an)elastic structure due to physical dispersion, affording orders of magnitude improvements in fits compared to earlier radial models of the core. REM1D is radially anisotropic in the upper mantle and is optimized to fit body-wave arrival times in agreement with widely used but theoretically incomplete isotropic models optimized for earthquake location (e.g., AK135). Historical estimates of core properties are broadly consistent with REM1D (Fig. 1); the strongest agreement (±0.2%) is on the depth of the core–mantle boundary at 3480 km while the gradients of velocities with depth and the related derivative properties (Fig. 1c) are most inconsistent due to limitations in past studies (Moulik and Ekström, 2025a).

Physical properties of the inner core derived from seismology have important implications for the temperature and composition of the Earth. Equations of state (EoS), which are used to calculate properties of minerals at high-pressure and temperature conditions (e.g., bulk

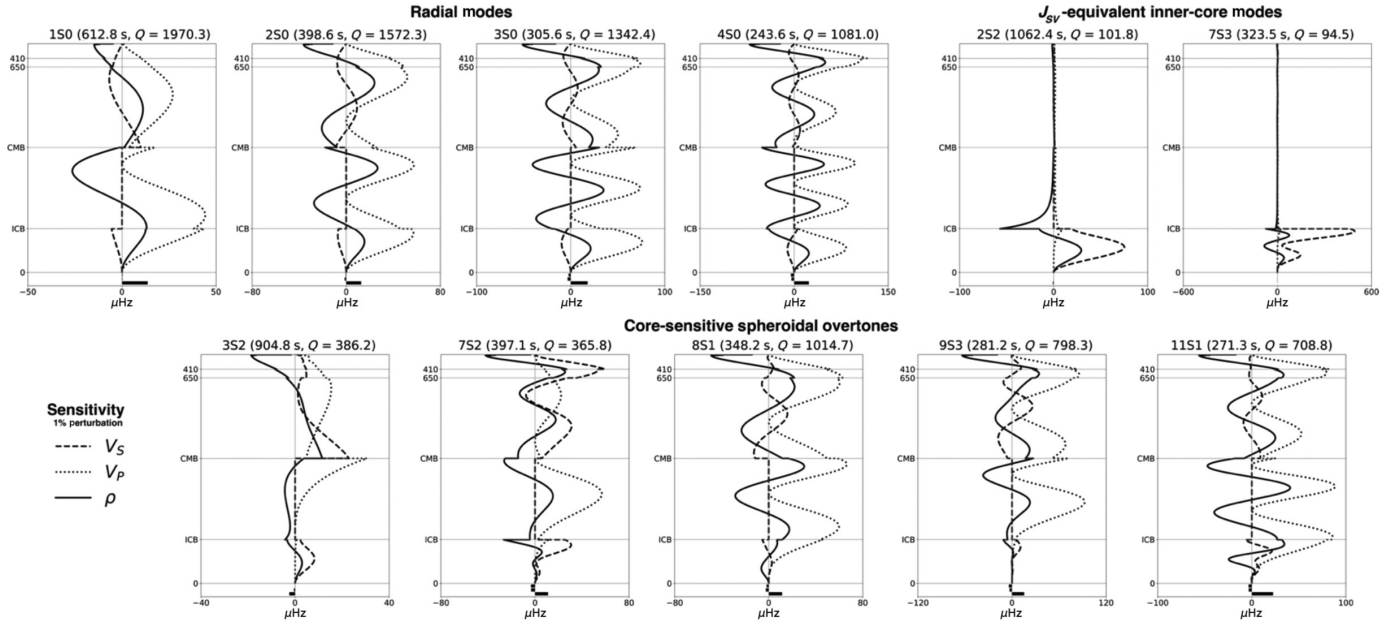

Figure 13. Sensitivity kernels of the inner-core sensitive modes employed by Dziewonski and Gilbert (1971). The kernels are calculated for perturbations of 1% using the radial REM1D (Moulik and Ekström, 2025a,b). The thick horizontal bars beneath the kernels show the mode's sensitivity (from top to bottom) to depth perturbations of the 410 and 650 km discontinuities and the core–mantle boundary. (a) Radial and (c) several spheroidal overtones are *PKIKP*-equivalent and afford V_P sensitivity. (b) J_{SV}-equivalent modes in the "real" Earth ($_2S_2$ and $_7S_3$) are primarily sensitive to V_S in the solid inner core and have not been measured; $_2S_2'$ and $_7S_3'$ in the fluid-core models correspond to $_3S_2$ and $_9S_3$ and have been measured (Table 2).

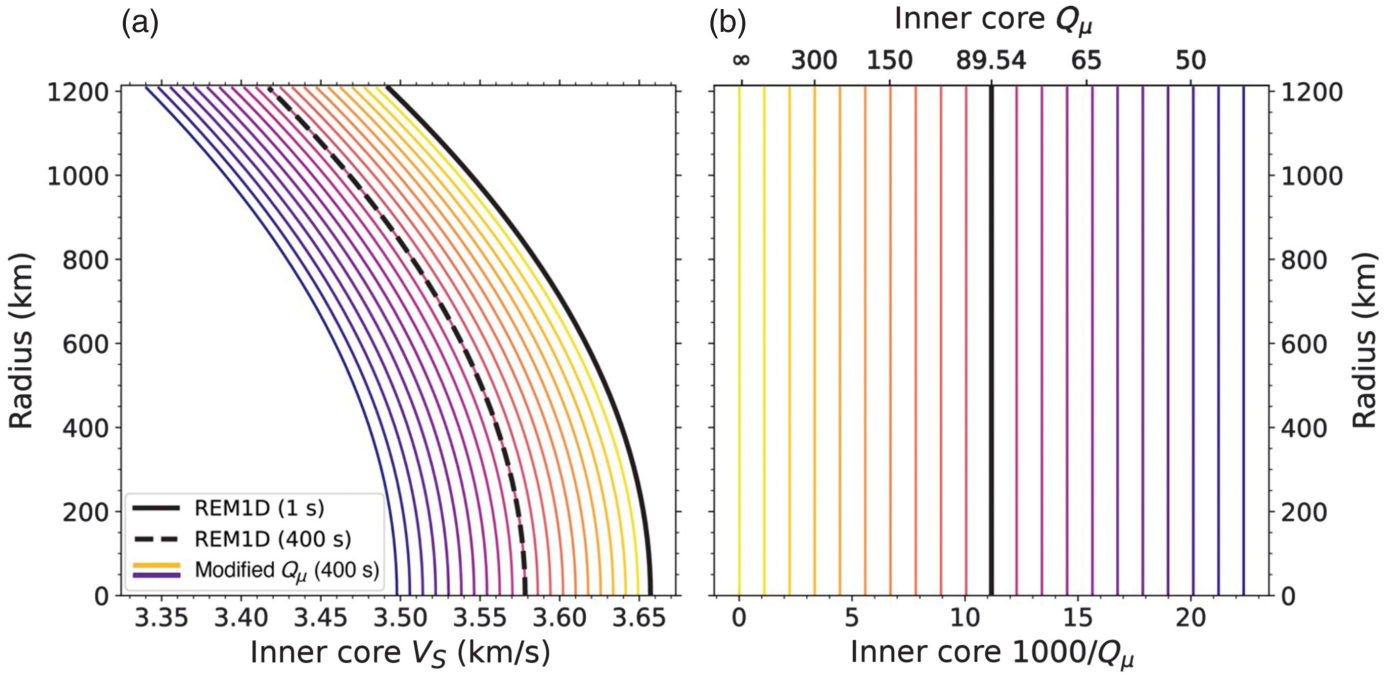

Figure 14. Various scenarios of shear dissipation in the (a,b) inner core. Low (and high) shear attenuation is marked by yellow (and purple) colors. Reference inner core $Q_\mu = 89.54$ and radially varying V_S profile from REM1D, defined at the reference period of 1 s are plotted as black curves. Because of the effects of physical dispersion, a perturbed V_S profile different from REM1D by up to ~150 m/s (black dashed curve) is "seen" by a typical core-sensitive mode at an eigenperiod ~400 s (Fig. 13). Physical dispersion allows the mode eigenperiods to provide additional constraints on the optimal Q_μ in the inner core (Fig. 15).

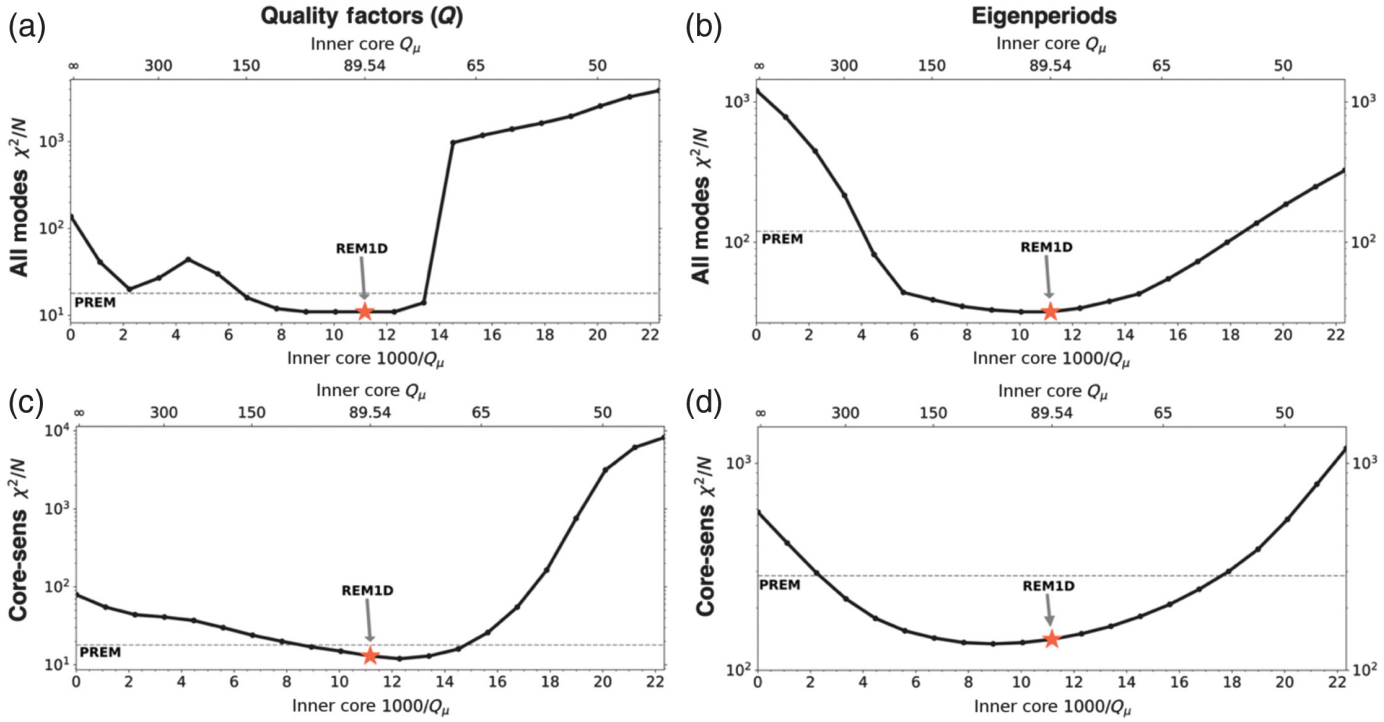

Figure 15. Evidence of strong shear dissipation in the inner core. Chi-square misfits are provided in semilog plots to all normal-mode quality factors (a,c) and eigenperiods (b,d), and the subset of core-sensitive modes (c,d) from the reference dataset, while accounting for the nonlinear crustal contributions to fundamental modes (Moulik and Ekström, 2025a,b). Perturbations are evenly spaced in $1000/Q_\mu$ relative to the REM1D inner-core $Q_\mu = 89.54$. REM1D fits all observations (red star) significantly better than PREM (gray dashed line). Note that the substantial changes in fits to eigenperiods are purely due to physical dispersion caused by shear dissipation (Fig. 14) because velocity/density structure is fixed at REM1D values.

modulus κ and its pressure derivative $\kappa' = d\kappa/dp$), are valid for an adiabatic region of uniform composition. Based on EoS predictions for a well-mixed isochemical region, the curvature κ'' should remain negative over the entire pressure range, decreasing in magnitude to zero at high pressures ($p \to \infty$) and therefore greater depths in a region of the Earth. REM1D removes the positive κ'' in the deepest ~1000 km of the outer core, which is an anomalous feature of PREM and body-wave models like AK135 (Fig. 1c). Deviations in earlier models were due to artifacts from parameterization and limitations of body-wave datasets (Moulik and Ekström, 2025a). EoS for various bulk compositions can be calibrated against seismological models, and past studies have argued for a solid inner core composed of a crystalline phase of iron with some light elements, and a liquid outer core comprising additional lighter alloying elements (e.g., C, H, S, Si, or O; Birch 1952, 1964; Jephcoat and Olson, 1987; Hirose *et al.*, 2013). REM1D finds κ' values in the inner core that are marginally higher (2.35–2.36) than PREM (2.33–2.34), which are features related to the 0.1%–0.5% reduction in velocities. The elastic and density variations in the REM1D inner and outer core follow closely the Adams–Williamson equation (e.g., stratification parameter $\eta_B = 1$; Bullen, 1963) with a negative κ'' throughout each region. Modern reference estimates of the physical properties are consistent with an iron-rich crystalline inner core and a neutrally stable outer core comprising a well-mixed iron alloy undergoing adiabatic compression (Moulik and Ekström, 2025b).

Discussion and Conclusion

We have revisited several historical studies that have helped shape our current understanding of the inner core from a seismological point of view. Although Oldham (1906) was able to identify a core, he did not speculate on its temperature or composition. It is possible that he misidentified the second phase as a late-arriving core phase instead of a bounce phase. Curiously, his data were biased toward late arrivals, which would suggest slower velocities than modern velocity models (Fig. 2). The problem of baseline differences in absolute arrivals and the overall slopes of teleseismic travel-time curves in early studies is well known. His observations were of limited quality and quantity (Muir and Tsai, 2020), and they likely contained errors in picking, earthquake time, and location. Although modern processing methods have improved earthquake characterization, leading to reduced baseline errors, discrepancies in arrival times across various filter bands and techniques persist and are being reconciled in collaboration with the seismological community (Moulik and The 3D Reference Earth Model [REM3D] Consortium, 2022).

In contrast to the data in Oldham (1906), we found that the data used by Lehmann (1936) and available in ISC (2025) for the

time span of 1904–1935 feature relatively accurate timing. If modern ray-tracing techniques were available, it would have been possible to estimate the inner core to within 2% with the entire dataset. Although there was a large spread in the historical data with a standard deviation of 4.03 s, we found relatively little systematic bias. Finally, we note that the modern phase arrival data are considerably more precise with a standard deviation of 1.83 s, and very accurate with a mean systematic deviation of 0.029 s, an order of magnitude better than the historical data spanning 1904–1935. Although this trend is an overall improvement for seismology, it does suggest that historical data cannot automatically be used for studying the interior of the Earth. Historical datasets would likely need to be digitally scanned so that new arrival times can be estimated with the high resolution afforded by modern scanners and the high consistency and reproducibility afforded by computer algorithms.

Although there is demonstrated value in scanning and digitizing historical seismic data, there are also several complications. For example, the simple task of scanning and digitizing these records will require a large effort (e.g., Alejandro *et al.*, 2018). Even after the scanning and digitization, it will be important to understand the timing quality of the records as well as the fidelity and quality of the scans and how these factors may be determined by how the data were recorded, written, and stored (Lee *et al.*, 2020, 2022). For example, errors may be related to historical operating practices, such as errors in the historical absolute-time corrections to clock drift made with radio time (e.g., Agnew, 2020), equipment, for example, nonlinear time drift caused by rotation changes in the drum or scanning errors (Lee *et al.*, 2023), or storage, for example, distortion of physical paper or film media that analog data are stored on over time (e.g., Lee *et al.*, 2022). Many of these records will also be complicated to analyze because of their time-varying responses and the lack of metadata in modern formats (Ringler *et al.*, 2020). Our analysis of the same stations used by Lehmann (1936) suggests that many of the large arrival residuals persist in modern records. Based on a ten-year window centered around 2000, the standard deviation of residuals generally decreases, but there can be substantial periods of time with large amounts of outlier data (Figs. 10 and 11). This suggests that scanning and digitizing a large number of records would likely be necessary because the spread of the residuals could be large and potentially biased if only a few stations are used. Despite current limitations in the timing and resolution of historical stations, such a change would accrue over decades and could potentially be detected with fidelity in long-term records (e.g., 1.07 s change in 100 yr). Such work is especially promising if the large spread in the residuals of stations (Fig. 11b) is reduced. Such a reduction in uncertainty may be achieved through the repicking of phases using modern resources and techniques because changes in median arrival times larger than 1 s over time may be due to errors in the original picks or instrumentation (e.g., Röhm *et al.*, 1999).

Historically, identification of normal-mode multiplets in digitized seismograms for radial structure was done with coarse sampling rates of ∼2–16 samples per second. However, a mode multiplet (and its constitutive singlets) may split due to Earth's heterogeneity and remain in resonance with other modes, resulting in complicated spectral signatures. Several inner-core sensitive normal modes are observed to split in a way that is consistent with a transversely isotropic inner core with a symmetry axis parallel to that of the Earth's rotation (e.g., Woodhouse *et al.*, 1986; Tromp, 1995). The estimation of splitting parameters from waveform spectra requires high-frequency resolution and timing accuracies in continuous time series (without gaps) spanning multiple hours and days (∼1.1 Q cycles per mode; Dahlen, 1982), a requirement that needs to be met during the digitization of historical records for this application. The Q cycle corresponds to the time required for the modal signal to decay by $e^{-\pi}$ and is defined as the quality factor Q of the mode multiplied by its eigenperiod in seconds. The processing for several higher-order overtones is often attempted after removing the first several (up to 15 or 20) hours of each seismogram to leverage the property of the Earth as an attenuation filter (e.g., Dratler *et al.*, 1971). This process removes the fundamental modes and other modes with shorter Q cycles that attenuate after the first few hours, but it also necessitates long records. So long as archives of historical seismograms continue to exist and remain accessible, expanding mode-splitting datasets with historical data may be a valuable prospect given that the methods by which historical analog data can be recovered and digitized have improved significantly in the last half-century (e.g., Ishii and Ishii, 2022).

Modern observational seismology leverages a combination of theoretical advancements in wave propagation and large-scale computational resources that were unthinkable at the time of the discovery and early physical characterization of the inner core. Nevertheless, there could still be value in many of the historical records used in these efforts because the quality of the data in certain respects is not substantially different than modern records. Although it may remain challenging to use these historical data for applications that require high precision ($\ll$1 s), their utility is clear for certain applications where an extended time record is necessary even with only coarse timing. For example, changes in ocean-generated microseism amplitudes can be investigated with the sampling rate of a minute and power spectral densities (Lecocq *et al.*, 2020). Finally, while modern observational seismology has come a long way with recent studies involving massive datasets (e.g., Moulik *et al.*, 2022), many of the fundamental observations that have improved our understanding of the Earth's interior were made using careful analysis of only a few records. The work of Lehmann (1936) fits into this category and was truly revolutionary for the era in which she worked. The combined analysis of historical records that provide invaluable temporal coverage in conjunction with the ever-expanding sets of

high-precision and high-accuracy observations from global seismographic networks may help detect new structural features of the Earth and refine previous estimates.

Based on the eigenfrequencies of normal modes, it is now well established that the inner core is solid. Although an inner core distinct in V_P structure was detected using *PKP* waves (Lehmann, 1936), it could only be validated as a solid region using the additional V_S and density sensitivity afforded by normal modes (Dziewonski and Gilbert, 1971). Two spheroidal overtones (${}_6S_1'$ and ${}_8S_1'$) were likely misidentified by this study, and discrepancies exist between the reported eigenperiods and modern reference estimates (Moulik and Ekström, 2025a). Nevertheless, the underlying conclusion holds true because the rigidity of the core provides the only way to jointly fit the eigenperiod observations of both radial modes and core-sensitive spheroidal overtones. Moreover, the strong shear dissipation in REM1D ($Q_\mu = 89.54$) affords a clear and optimal fit to the modern reference datasets of mode eigenperiods and quality factors accounting for physical dispersion. Because a liquid region would only have bulk dissipation, the narrow range of low Q_μ estimates from reference datasets supports the earlier conclusion based on eigenperiods alone that the inner core is solid (Dziewonski and Gilbert, 1971, 1972). Although several articles have reported observations of shear body-wave phases through the inner core, these observations are difficult to make because of their small amplitudes and interactions with other incoming phases arriving simultaneously.

Despite the limitations of theory and computational resources at the time, early seismological studies fundamentally shaped our understanding of the Earth's interior and motivated new research. Although the availability of data was limited in historical studies, it was adequate to discern the first-order features, and gross errors in early studies are remarkably low. Modern estimates of the average physical properties in the inner core are reported by the radial REM1D (Fig. 1; Moulik and Ekström, 2025a,b). The inner core is now considered a region 1215 km in radius with nonzero, radially varying shear and compressional velocities, and a strong, uniform shear attenuation ($Q_\mu = 89.54$). Reconciliation of historical and modern seismological datasets holds immense promise for future discoveries on inner-core structure.

Data and Resources

The reference dataset, radial reference Earth model (REM1D; Moulik and Ekström, 2025a,b), and codes to evaluate physical parameters at arbitrary locations are available from the project webpage (http://rem3d.org, last accessed August 2025) and are permanently archived on Zenodo (doi: 10.5281/zenodo.8407693; Moulik, 2025). Normal-mode calculations accounting for new astronomic–geodetic constants and ray tracing through both anisotropic (e.g., REM1D) and isotropic models (e.g., AK135) were performed using the open-source AVNI toolkit (http://avni.globalseismology.org, last accessed July 2025; Moulik *et al.*, 2023), which extends the anisotropic formulations of Woodhouse (1981, 1988). Code to reproduce all other figures will be published at https://code.usgs.gov/asl/papers/ringler (last accessed July 2025). The authors made extensive use of the Python packages Matplotlib (Hunter, 2007), ObsPy (Megies *et al.*, 2011), and Cartopy (Met Office, 2015). This work was supported by the Gordon and Betty Moore Foundation Award GBMF12801 (doi: 10.37807/GBMF12801).

Declaration of Competing Interests

The authors acknowledge that there are no conflicts of interest recorded.

Acknowledgments

The authors thank an anonymous reviewer, Duncan Agnew, Kristen Marra, Guust Nolet, and Brian Shiro for helpful reviews that improved this article. The authors also thank Paul Richards for reviewing this work and suggesting a number of additional pieces focused on body-wave observations. This work benefited from an early review by Paul Earle. The authors thank Duncan Agnew for providing several historical references that helped in the identification of stations as well as answering many questions. The authors thank Guy Masters, Fredrick Pollitz, Frederik Simons, and Joe Steim for helping track down some of the normal-mode frequencies. The authors thank Tyler Storm for providing several PKP_{df} phase examples. Adam T. Ringler supported the initial conception, formal analysis, data curation, visualization, writing—original draft, and writing—reviewing and editing. Pritwiraj Moulik supported the data curation, formal analysis, visualization, methodology, writing—original draft, and writing—reviewing and editing. Thomas L. Lee supported the methodology, writing—original draft, and writing—reviewing and editing. David C. Wilson supported the methodology, writing—original draft, and writing—reviewing and editing. Robert E. Anthony supported the methodology, writing—original draft, and writing—reviewing and editing.

References

Agnew, D. C. (2020). Time marks and clock corrections: A century of seismological timekeeping, *Seismol. Res. Lett.* **91,** no. 3, 1417–1429, doi: 10.1785/0220190284.

Aki, K., and P. Richards (2002). *Quantitative Seismology: Second Edition*, University Science Books, Sausalito, 700 pp.

Alejandro, A. C. B., C. R. Hutt, A. T. Ringler, S. V. Moore, R. E. Anthony, and D. C. Wilson (2018). The Albuquerque Seismological Lab WWSSN film chip preservation project, *Seismol. Res. Lett.* **90,** no. 1, 401–408, doi: 10.1785/0220180275.

Anderssen, R. S., and J. R. Cleary (1980). Estimation of *PKP* times from ISC data, *Phys. Earth Planet. Int.* **23,** 207–214, doi: 10.1016/0031-9201(80)90110-7.

Backus, G., and F. Gilbert (1968). The resolving power of gross Earth data, *Geophys. J. Int.* **16,** no. 2, 169–205, doi: 10.1111/j.1365-246X.1968.tb00216.x.

Birch, F. (1940). The alpha-gamma transformation of iron at high pressures, and the problem of the Earth's magnetism, *Am. J. Sci.* **238,** no. 3, 192–211, doi: 10.2475/ajs.238.3.192.

Birch, F. (1952). Elasticity and constitution of the Earth's interior, *J. Geophys. Res.* **57,** no. 2, 227–286, doi: 10.1029/JZ057i002p00227.

Birch, F. (1964). Density and composition of mantle and core, *J. Geophys. Res.* **69,** no. 20, 4377–4388, doi: 10.1029/jz069i020p04377.

Bolt, B. A. (1982). *Inside the Earth: Evidence from Earthquakes*, W. H. Freeman and Company, New York, 191 pp., doi: 10.1016/0191-8141(83)90063-9.

Bormann, P., D. A. Storchak, and J. Schweitzer (2013). The IASPEI standard nomenclature of seismic phases, in *New Manual of Seismological Observatory Practice 2*, Geutsches GeoForschungsZentrum GFAZ, Potsdam, Germany, 20 pp., doi: 10.2312/GFZ.NMSOP-2_IS_2.1.

Brekhovskikh, L. M. (1960). *Waves in Layered Media*, Academic Press, London, 561 pp.

Brush, S. G. (1980). Discovery of the Earth's core, *Am. J. Phys.* **48,** 705–724, doi: 10.1119/1.12026.

Buffet, B. A. (1996). A mechanism for decade fluctuations in the length of day, *Geophys. Res. Lett.* **23,** no. 25, 3803–3806, doi: 10.1029/96GL03571.

Buland, R., and C. H. Chapman (1983). The computation of seismic travel times, *Bull. Seismol. Soc. Am.* **73,** no. 5, 1271–1302, doi: 10.1785/BSSA0730051271.

Bullen, K. E. (1950). Theoretical travel-times of S waves in the Earth's inner core, *Geophys. J. Int.* **6,** no. s2, 125–128, doi: 10.1111/j.1365-246X.1950.tb02986.x.

Bullen, K. E. (1963). An index of degree of chemical inhomogeneity in the earth, *Geophys. J. Int.* **7,** no. 5, 584–592, doi: 10.1111/j.1365-246X.1963.tb03823.x.

Burdick, S., L. Waszek, and V. Lekić (2019). Seismic tomography of the uppermost inner core, *Earth Planet. Sci. Lett.* **528,** 115,789, doi: 10.1016/j.epsl.2019.115789.

Cormier, V. F., M. I. Bergman, and P. L. Olson (2021). *Earth's Core: Geophysics of a Planet's Deepest Interior*, Elsevier, Amsterdam, The Netherlands, 324 pp.

Crotwell, H. P., T. J. Owens, and Ritsema (1999). The TauP toolkit: Flexible seismic travel-time and ray-path utilities, *Seismol. Res. Lett.* **70,** no. 2, 154–160, doi: 10.1785/gssrl.70.2.154.

Dahlen, F. A. (1982). The effect of data windows on the estimation of free oscillation parameters, *Geophys. J. Int.* **69,** no. 2, 537–549, doi: 10.1111/J.1365-246X.1982.tb04964.x.

Dahlen, F. A., and J. Tromp (1998). *Theoretical Global Seismology*, Princeton University Press, New Jersey, 1025 pp., doi: 10.2307/j.ctv131bvfd.

Deuss, A. (2014). Heterogeneity and anisotropy of Earth's inner core, *Annu. Rev. Earth Planet. Sci.* **42,** 103–126, doi: 10.1146/annurev-earth-060313-054658.

Dratler, J., W. E. Farrell, B. Block, and F. Gilbert (1971). High-Q overtone modes of the Earth, *Geophys. J. Int.* **23,** no. 4, 399–410, doi: 10.1111/j.1365-246X.1971.tb01832.x.

Dziewonski, A. M., and D. L. Anderson (1981). Preliminary reference Earth model, *Phys. Earth Planet. Inter.* **25,** no. 4, 297–356, doi: 10.1016/0031-9201(81)90046-7.

Dziewonski, A. M., and F. Gilbert (1971). Solidity of the inner core of the Earth inferred from normal mode observations, *Nature* **234,** no. 5330, 465–466, doi: 10.1038/234465a0.

Dziewonski, A. M., and F. Gilbert (1972). Observations of normal modes from 84 recordings of the Alaska earthquake of 1964 March 28, *Geophys. J. Int.* **27,** no. 4, 393–446, doi: 10.1111/j.1365-246X.1972.tb06100.x.

Gutenberg, B. (1913). Über die konstituion des Erdinnern, erschlossen aus Erdbebenbeobachtungen, *Z. Geophys.* **14,** 1217–1218 (in German).

Gutenberg, B., and C. F. Richter (1938). P′ and the Earth's core, *Geophys. Suppl. Mon. Notices Roy. Astron. Soc.* **4,** no. 5, 363–372, doi: 10.1111/J.1365-246X.1938.tb01761.x.

Hirose, K., S. Labrosse, and J. Hernlund (2013). Composition and state of the core, *Annu. Rev. Earth Planet. Sci.* **41,** 657–691, doi: 10.1146/annurev-earth-050212-124007.

Hunter, J. D. (2007). Matplotlib: A 2D graphics environment, *Comput. Sci. Eng.* **9,** no. 3, 90–95, doi: 10.1109/MCSE.2007.55.

International Seismological Centre (ISC) (2025). *Online bulletin*, doi: 10.31905/D808B830.

Ishii, M., and H. Ishii (2022). DigitSeis: Software to extract time series from analogue seismograms, *Progr. Earth Planet. Sci.* **9,** no. 1, 50, doi: 10.1186/s40645-022-00508-0.

Jeans, J. (1927). The propagation of earthquake waves, *Proc. Math. Phys. Sci.* **102,** 554–574, doi: 10.1098/rspa.1923.0015.

Jeffreys, H. (1926). The rigidity of the Earth's central core, *Geophys. Suppl. Mon. Notices Roy. Astron. Soc.* **1,** 371–383, doi: 10.1111/j.1365-246X.1926.tb05385.x.

Jeffreys, H., and K. E. Bullen (1940). *Seismological Tables, British Association for the Advancement of Science*, Gray Milne Trust, London, 50 pp.

Jephcoat, A., and P. Olson (1987). Is the inner core of the Earth pure iron?, *Nature* **325,** no. 6102, 332–335, doi: 10.1038/325332a0.

Kennett, B. L. N., E. R. Engdahl, and R. Buland (1995). Constraints on seismic velocities in the Earth from traveltimes, *Geophys. J. Int.* **122,** no. 1, 108–124, doi: 10.1111/j.1365-246X.1995.tb03540.x.

Kölbl-Ebert, M. (2001). Inge Lehmann's paper: "P′" (1936), *Episodes* **24,** 262–267, doi: 10.18814/epiiugs/2001/v24i4/007.

Krasnoshchekov, D. N., P. B. Kaazik, and V. M. Ovtchinnikov (2005). Seismological evidence for mosaic structure of the surface of the Earth's inner core, *Nature* **435,** 483–487, doi: 10.1038/nature03613.

Lecocq, T., F. Ardhuin, F. Collin, and T. Camelbeeck (2020). On the extraction of microseismic ground motion from analog seismograms for the validation of ocean-climate models, *Seismol. Res. Lett.* **91,** no. 3, 1518–1530, doi: 10.1785/0220190276.

Lee, T., M. Ishii, and P. Okubo (2020). Relative time corrections for historical analog seismograms using the single-day ambient noise correlation function, *Bull. Seismol. Soc. Am.* **110,** no. 6, 3185–3195, doi: 10.1785/0120190313.

Lee, T., M. Ishii, and P. Okubo (2022). Assessing the fidelity of seismic records from microfilm and paper media, *Seismol. Res. Lett.* **93,** no. 6, 3444–3453, doi: 10.1785/0220220134.

Lee, T. A., A. T. Ringler, R. E. Anthony, and M. Ishii (2023). Comparison of corecorded analog and digital systems for characterization of responses and uncertainties, *Seismol. Res. Lett.* **94,** no. 5, 2301–2312, doi: 10.1785/0220230129.

Lehmann, I. (1936). P′, *Bureau Central Seismol. Int.* **14,** 87–115.

Megies, T., M. Beyreuther, R. Barsch, L. Krischer, and J. Wassermann (2011). ObsPy – What can it do for data centers and observatories?, *Ann. Geophys.* **54,** no. 1, 47–58, doi: 10.4401/ag-4838.

Met Office (2015). Cartopy: A cartographic Python library with a Matplotlib interface, Exter, Devon, available at http://scitools.org.uk/cartopy (last accessed October 2019).

Mochizuki, E. (1986). The free oscillations of an anisotropic and heterogeneous Earth, *Geophys. J. Int.* **86,** no. 1, 167–176, doi: 10.1111/j.1365-246X.1986.tb01078.x.

Moulik, P. (2025). Dataset and software for the radial reference earth model REM1D, *Phys. Earth Planet. Int. (v1.0). Zenodo*, doi: 10.5281/zenodo.8407693.

Moulik, P., and , and The 3D Reference Earth Model (REM3D) Consortium (2022). *Three Dimensional Reference Earth Model Project: Data, Techniques, Models & Tools*, American Geophysical Union Fall Meeting, Chicago, Illinois, doi: 10.5281/zenodo.7883683.

Moulik, P., and G. Ekström (2025a). Radial structure of the Earth: [I] Model concepts and data, *Phys. Earth Planet. Int.* pp. 1–123, 107,319, doi: 10.1016/j.pepi.2025.107319.

Moulik, P., and G. Ekström (2025b). Radial structure of the Earth: [II] Model features and interpretations, *Phys. Earth Planet. Int.* 107,320, doi: 10.1016/j.pepi.2025.107320.

Moulik, P., V. Lekic, B. Romanowicz, Z. Ma, A. Schaeffer, T. Ho, E. Beucler, D. Debayle, A. Deuss, S. Durand, *et al.* (2022). Global reference seismological data sets: Multimode surface wave dispersion, *Geophys. J. Int.* **228,** no. 3, 1808–1849, doi: 10.1093/gji/ggab418.

Moulik, P., R. Maguire, R. Gassmoeller, and C. Havlin (2023). AVNI: Analysis and visualization toolkit for planetary inferences, doi: 10.5281/zenodo.10035731.

Muir, J. B., and V. C. Tsai (2020). Did Oldham discover the core after all? Handing imprecise historical data with hierarchical Bayesian model selection methods, *Seismol. Res. Lett.* **91,** no. 3, 1377–1383, doi: 10.1785/0220190266.

Okal, E., and Y. Cansi (1998). Detection of *PKJKP* at intermediate periods by progressive multi-channel correlation, *Earth Planet. Sci. Lett.* **164,** 23–30, doi: 10.1016/S0012-821X(89)00210-6.

Oldham, R. D. (1906). The constitution of the interior of the Earth, as revealed by earthquakes, *Q. J. Geol. Soc.* **62,** 456–475, doi: 10.1144/GSL.JGS.1906.062.01-04.21.

Peterson, J, and C. R. Hutt (2014). World-wide standardized seismograph network—A data users guide, *U.S. Geol. Surv. Open-File Rept. 2014-1218* , 74 pp., doi: 10.3133/ofr20141218.

Richards, P. G. (2000). Earth's inner core-discoveries and conjectures, *Astron. Geophys.* **41,** no. 1, 1.20–1.24, doi: 10.1046/j.1468-4004-2000.00020.x.

Ringler, A. T., R. E. Anthony, D. C. Wilson, D. Auerbach, S. Bargabus, P. Davis, M. Gunnels, K. Hafner, J. F. Holland, A. Kearns, and E. Klimczak (2021). A review of timing accuracy across the Global Seismographic Network, *Seismol. Res. Lett.* **92,** no. 4, 2270–2281, doi: 10.1785/0220200394.

Ringler, A. T., D. C. Wilson, E. Wolin, T. Storm, and L. Sandoval (2020). Calibration analysis and noise estimates of WWSSN station ALQ (Albuquerque, New Mexico), *Seismol. Res. Lett.* **91,** no. 3, 1359–1366, doi: 10.1785/0220190201.

Röhm, A. H. E., J. Trampert, H. Paulssen, and R. K. Snider (1999). Bias in reported seismic arrival times deduced from the ISC Bulletin, *Geophys. J. Int.* **137,** no. 1, 163–174, doi: 10.1046/j.1365-246x.1999.00774.x.

Shearer, P. M., C. A. Rychert, and Q. Liu (2011). On the visibility of the inner-core shear wave phase PKJKP at long periods, *Geophys. J. Int.* **185,** 1379–1383, doi: 10.1111/j.1365-246X.2011.05011.x.

Song, X., and P. G. Richards (1996). Seismological evidence for differential rotation of the Earth's inner core, *Nature* **382,** no. 6588, 221–224, doi: 10.1038/382221a0.

Souriau, A., and M. Calvet (2015). Deep Earth structure: The Earth's core, in *Treatise on Geophysics*, Second Ed., G. Schubert (Editor), Vol. 1, Elsevier, Amsterdam, The Netherlands, 655–693, doi: 10.1016/B978-0-444-53802-4.00020-8.

Tkalčić, H. (2017). *The Earth's Inner Core Revealed by Observational Seismology*, Cambridge University Press, Cambridge, 234 pp., doi: 10.1017/0781139583954.

Tkalčić, H. (2024). On the inner-core differential-rotation (un)resolvability from earthquake doublets: The traps of data selection, *Geophys. Res. Lett.* **51,** no. 6, e2023GL107043, doi: 10.1029/2023GL107043.

Tkalčić, H., S. Wang, and T. -S. Phan (2022). Shear properties of Earth's inner core, *Annu. Rev. Earth Planet. Sci.* **50,** 153–181, doi: 10.1146/annurev-earth-071521-063942.

Tromp, J. (1995). Normal-mode splitting due to inner-core anisotropy, *Geophys. J. Int.* **121,** no. 3, 963–968, doi: 10.1111/j.1365-246X.1995.tb06451.x.

Waszek, L., and A. Deuss (2013). A low attenuation layer in the Earth's uppermost inner core, *Geophys. J. Int.* **195,** no. 3, 2005–2015, doi: 10.1093/gji/ggt368.

Widmer, R., G. Masters, and F. Gilbert (1991). Spherically symmetric attenuation within the Earth from normal mode data, *Geophys. J. Int.* **104,** no. 3, 541–553, doi: 10.1111/j.1365-246X.1991.tb05700.x.

Wood, H. O. (1921). A list of seismologic stations of the world, *Bull. Natl. Res Counc.* **2,** no. 15, 397–538.

Woodhouse, J. (1988). The calculation of the eigenfrequencies and eigenfunctions of the free oscillations of the earth and the sun, in *Seismological Algorithms: Computational Methods and Computer Programs*, D. J. Doornbos (Editor), Academic Press, San Diego, California, pp. 321.

Woodhouse, J. H. (1976). On Rayleigh's principle, *Geophys. J. Int.* **46,** no. 1, 11–22, doi: 10.1111/j.1365-246X.1976.tb01629.x.

Woodhouse, J. H. (1981). A note on the calculation of travel times in a transversely isotropic Earth model, *Phys. Earth Planet. Int.* **25,** no. 4, 357–359, doi: 10.1016/0031-9201(81)90047-9.

Woodhouse, J. H., D. Giardini, and X. -D. Li (1986). Evidence for inner core anisotropy from free oscillations, *Geophys. Res. Lett.* **13,** no. 13, GL013i013p01549, 1549–1552, doi: 10.1029/GL013i013p01549.

Manuscript received 24 February 2025
Published online 10 September 2025